Polarimetric Temporal Analysis of Urban Environments With a Ground-Based SAR

Luca Pipia, Xavier Fabregas, *Member, IEEE*, Albert Aguasca, and Carlos López-Martínez, *Senior Member, IEEE*

***Abstract*—Revisiting time constitutes a key constraint for continuous monitoring activities based on space- and airborne synthetic aperture radar (SAR) acquisitions. Conversely, the employment of terrestrial platforms overcomes this limitation and makes it possible to perform time-continuous observations of small space-scale phenomena. New research lines of SAR dealing with the backscattering evolution of different types of scenarios become hence possible through the analysis of ground-based SAR (gbSAR) data collections. The Remote Sensing Laboratory of the Universitat Politècnica de Catalunya drove a one-year measurements campaign in the village of Sallent, northeastern Spain, using its X-Band gbSAR sensor. The field experiment aimed at studying the subsidence phenomenon induced by the salt mining activity carried out in this area during the past decades. In this paper, the polarimetric behavior of an urban environment is investigated at different time scales. After a brief description of the test site and the measurement campaign, the analysis is focused on the stability on man-made structures at different time scales. PolSAR data monthly acquired from June 2006 to July 2007 are employed to stress the presence of nonstationary backscattering processes within the urban scene and the effect they have on differential phase information. Then, a filtering procedure aiming at reducing backscattering randomness in one-day and long-term data collections is then put forward. The improvements provided by the proposed technique are assessed using a new polarimetric descriptor, the time entropy. In the end, the importance of preserving the interferometric phase information from nonstationary backscattering contaminations using fully polarimetric data is discussed.**

***Index Terms*—Ground-based synthetic aperture radar (gbSAR) systems, polarimetric entropy, radar polarimetry.**

I. Introduction

THE USE of spaceborne synthetic aperture radar (SAR) systems is extremely successful for the study of the evolution of slow processes over wide areas. Yet, it may be unsuitable when high flexibility in terms of revisiting time is needed, as to foresee possible hazard conditions. In an attempt to overcome this limitation, during the last years, the research activity of several remote sensing groups was devoted to the development of terrestrial SAR systems. Easy to deploy, extremely cheaper if compared to spaceborne solutions, ground-based SAR (gbSAR) sensors represent a cost-effective solution for the continuous monitoring of small-scale phenomena. Briefly, these systems consist of a continuous-wave radar [1], [2] mounted on a sliding support and synthesizing in time an aperture longer than the physical dimension of their real antennas. They merge the SAR capability to obtain 2-D reflectivity images and the advantages offered by a terrestrial platform, namely high stability, perfect knowledge of sensor's track, and absence of any revisiting time constrain.

The Remote Sensing Laboratory (RSLab), at the Universitat Politècnica de Catalunya (UPC), operates a polarimetric gbSAR sensor [3]. Instead of using a vector network analyzer (VNA) to synthesize a stepped-frequency bandpass signal at each position of the rail, the RSLab devised a specific hardware based on a direct digital synthesizer that optimizes, in terms of time, the processes of signal generation and transmission. It follows that the time required for the scanning process shortens significantly with respect to any VNA-based solutions. Owing to its performances, the RSLab sensor was contacted by the Institut Geològic de Catalunya for a one-year measuring campaign in the village of Sallent, in northeastern Spain.

The village of Sallent is located within the Llobregat River Depression, a basin made of a great saline unit composed by potash salts alternating layers. The potash salts were traditionally exploited since ancient times and are still an important mining activity in the region. The Enrique mine of Sallent was under exploitation until 1974. In 1954, a natural cavity of about 120 m high and 40 m wide was found during mining works under the southeast district of the village, known as the Station district or *Barri de l'Estació*, close to the Llobregat River. Water floods in 1957 and 1962 forced to abandon this part of the mine, filling up the cavity with saturated salty water. During the 1990s, heavy damages appeared in man-made structures built within the district. As a response, the Catalan Administration started a research program to identify, quantify, and model the subsidence phenomena in this area [4]. In the framework of that program, a multiple set of techniques, such as topographic leveling, geological mapping, geophysic prospection, extensometric measurements, drilling, and orbital DInSAR, were employed to evaluate the risk of structure collapse [4]. In 2003, the SAR group of the UPC, jointly with the Institut Cartografic de Catalunya, studied the geological behavior of the district applying DInSAR techniques to ERS-1/2 acquisitions [5]. A new collaboration between the two institutions started at the end of June 2006 as an attempt to improve both the spatial accuracy and temporal sampling of the deformation process using the UPC gbSAR sensor.

Manuscript received December 27, 2011; revised June 20, 2012 and July 13, 2012; accepted July 15, 2012. This work was supported by the Institut Geologic de Catalunya (IGN) and the Spanish Ministerio de Ciencia e Innovación, under projects TEC2008-06764-C02-01 (Feder Funds) and TEC2011-28201-C02-01.

L. Pipia is with the Institut Cartogràfic de Catalunya, 08038 Barcelona, Spain.

X. Fabregas, A. Aguasca, and C. López-Martínez are with the Department of Signal Theory and Communications, Universitat Politècnica de Catalunya, 08034 Barcelona, Spain.

Color versions of one or more of the figures in this paper are available online at http://ieeexplore.ieee.org.

Digital Object Identifier 10.1109/TGRS.2012.2211369

(a) (b)

Fig. 1. (a) UPC ground-based SAR sensor and (b) wide-angle view of the test-site from the its location in Sallent.

In this paper, PolSAR data acquired during approximately one year are employed to perform an in-depth analysis of the polarimetric behavior of urban environments at different time scales. After a brief description of the test site and the measuring campaign, the temporal stability of urban targets during one-day monitoring activity is analyzed. Single-polarization- and polarimetric-based descriptors are employed to demonstrate that misleading phase information may be extracted from PolSAR data unless the temporal consistency of target polarimetric properties is previously assessed. After considering the daily measurements in a separate way, the analysis is then extended to long-term PolSAR series. The presence of polarimetric time patterns, which repeat in time, are employed to propose a filtering procedure selecting reliable, long-term, sample subsets guaranteeing backscattering stability at pixel level. A novel polarimetric descriptor, the time Entropy, is put forward as a trustworthy tool for the assessment of the filtering technique. First demonstrations of the high potential of polarimetry for deformation map retrieval with respect to single polarization approaches have been provided in [6] and [7]. In the conclusions, the importance of checking the stability of scatterers' polarimetric response in order to achieve further improvements in the accuracy of the differential phase estimation and, hence, in long-term differential applications is discussed.

II. Sensor Placement and Urban Environment Polarimetric Main Features

When a terrestrial radar solution is adopted for monitoring purposes, its location becomes a critical issue: the steeper the incidence angle, the higher the reduction of the shadowing effects, and the higher the sensitivity to subsidence. After a careful analysis of Sallent surroundings, the top of the cliff at the east side of the Station district was identified as the gbSAR best position. The observation angle of the area of interest varied from 72° up to 82°, and no radar front-end saturation was experienced due to the absence of close targets, as it can be observed in Fig. 1(a) and (b). The measurement campaign started in June 2006 and finished in July 2007. Table I describes the sensor setting parameters during the campaign, whereas Table II sums up the days chosen for the acquisition process, the amount of data sets daily gathered by the sensor, and the time span of consecutive data. Red color denotes diurnal monitoring activities whereas the nocturnal ones are indicated by the blue color. An example of the district reflectivity response in the horizontal transmit horizontal receive polarization combination (hh) is displayed in Fig. 2. Data calibration was carried out using a corner reflector located in a near-range bare area and a strong cross-polar urban target [8], [9]. A brief description of the main scattering mechanisms characterizing the urban environment is given by Pauli's decomposition. Accordingly, the scattering matrix $[S]$ measured by the gbSAR in the horizontal (h) vertical (v) linear polarization basis is decomposed into a trihedral-like, a dihedral-like, and 45°-tilted dihedral-like (or volumetric scattering in case of distributed target) components,

TABLE I
UPC gbSAR Measurement Parameters During the Campaign in Sallent

UPC gbSAR System	
Frequency Carrier f0	9.65 *GHz*
Chirp duration	50e-6 *sec*
Chirp Sampling Frequency	81.92 *MHz*
Chirp PRF	20 *Khz*
Chirp Bandwidth	[60:120] *MHz*
Deramped Signal Bandwidth	40 *MHz*
Transmitted Power	27 *dBm*
3dB Antenna Beamwidth	27º
Range Time-Average Factor	128
Synthetic Aperture Length	2 *m*
Cross-Range Samples	1 *cm*
Acquisition Duration: Single-Pol / PolSAR / PolInSAR	1 min / 2 min 40 sec / 4 min 30 sec

TABLE II
Timetable of the Measurement Campaign. Red and Blue Colors Denote the Diurnal and Nocturnal Measurements, Respectively

	Date	Time	# of Scans	Time-Delay
DAY 1	29/06/06	11:00-15:50	27	10 min
DAY 2	26/07/06	7:11-11:24	30	13 min
DAY 3	19/09/06	10:17-16:26	39	8 min
DAY 4	20/10/06	9:11-14:04	31	7 min
DAY 5	14/11/06	11:29-15:17	41	8 min
DAY 6	28-29/11/06	17:42-8:43	44	20 min
DAY 7	18-19/12/06	16:45-8:50	99	10 min
DAY 8	13-14/02/07	18:14-10:44	37	25 min
DAY 9	14-15/03/07	17:19-9:48	41	25 min
DAY 10	4-5/07/07	19:33-10:51	45	20 min

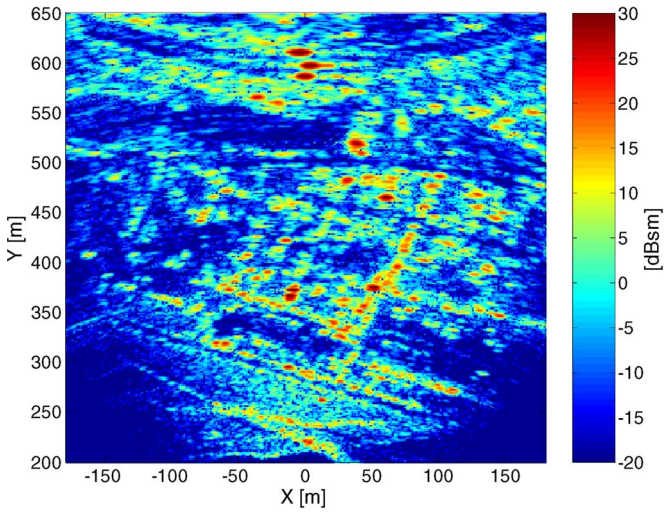

Fig. 2. Reflectivity image of the Station district of Sallent in the hh polarization in dBsm.

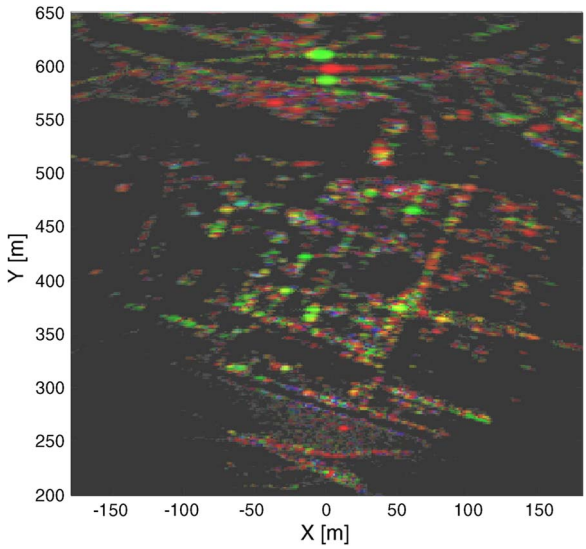

Fig. 3. RGB composition of Pauli's components within the Station district of Sallent weighted by span.

here denoted with a_T, a_D, and a_V. An example of an RGB composition of these three quantities (red for a_T, green for a_D, blue for a_V), after normalization by the span is shown in Fig. 3. The main advantage of the normalized Pauli components (NPCs) is their being insensitive to amplitude and phase global offsets. Observing Fig. 3, it can be noticed that one dominant mechanism characterizes most of the pixels. Red and green pixels are mainly detectable. Few yellow points, describing the concurrent presence of both single and double bounces, are observable too. Blue points, which are quite rare, are generated by multiple-reflections phenomena. The polarimetric features of the monitored scenario agree perfectly with the results obtained with other SAR platforms: man-made structures are mainly characterized by strong dihedral-like scattering generated by the interaction between vertical elements, i.e., walls, and the ground [10], [11]. Even if these studies were based on the analysis of L-band and X-band airborne SAR acquisitions, the analogies shown by gbSAR observations make it possible to extend these general considerations to terrestrial platforms. Yet, the weight that the dielectric constant might assume at high incidence ($> 70°$) in terms of geometrical interpretation of the Pauli's components will be carefully looked into in Appendix A.

III. Urban Environment Daily Stability

The scattering matrix measured by the UPC sensor, under the hypothesis of propagation through a homogenous medium, may be defined as [12]

$$[S'] = \begin{bmatrix} S_{hh} & S_{hv} \\ S_{hv} & S_{vv} \end{bmatrix} e^{-j2k_0 n_t r} + [N_T] \tag{1}$$

being r the target range position, n_t the troposphere refractive index, k the wavenumber, and $[N_T]$ a 2×2 complex matrix accounting for the additive noise contribution. Note that the main assumption in (1) is that n_t is constant during the time required for the aperture synthesis, i.e., gbSAR acquisitions are considered instantaneous.

Let w define one of the measurement dates reported in Table II and N_w the corresponding number of zero-baseline data sets gathered by the gbSAR system in that day. The expression describing the ith scattering matrix of the collection may be rewritten as

$$[S']_i^w = \begin{bmatrix} S_{hh}^{i,w} & S_{hv}^{i,w} \\ S_{hv}^{i,w} & S_{vv}^{i,w} \end{bmatrix} e^{-j2k_0(n_{1,w}+\Delta n_{i,w})r} + [N_T]_i^w, \quad i = 1, \ldots, N_w \tag{2}$$

where $n_{1,w}$ is the refractive index of the first acquisition (master) and $\Delta n_{i,w}$ describes the variation of the propagation properties due to changes of the troposphere in data set i with respect to the master image. It is worth recalling that changes of the refractive index generate interferometric phase variations among zero-baseline data sets that are proportional to the target-to-sensor range distance, as it was demonstrated in [12]. If no deformation process has taken place between the two acquisitions, high-coherence pixels may be used for the estimation of this undesired contribution by fitting their interferometric phase information to a range linear model [12].

After compensating for the corresponding atmospheric-induced phase ramps, the ith scattering matrix of the gbSAR daily collection becomes

$$\widehat{[S']}_i^w = \begin{bmatrix} S_{hh}^{i,w} & S_{hv}^{i,w} \\ S_{hv}^{i,w} & S_{vv}^{i,w} \end{bmatrix} e^{-j2k_0 n_{1,w} r} + [N_T]_i^w, \quad i = 1, \ldots, N_w. \tag{3}$$

In the case of time-invariant deterministic scatterers, $\widehat{[S']}_i^w$ is constant over time and depends only on their position with respect to the sensor. This behavior is typical of speckle-free scatterers and generally associated with pixels belonging to urban structures [13]. Despite this assumption is widely shared in the SAR remote sensing community, the analysis of real X-band gbSAR data reveals that this hypothesis might be unfulfilled. That is, the evolution of the amplitude A and absolute phase φ of the different polarimetric channels within the Sallent urban

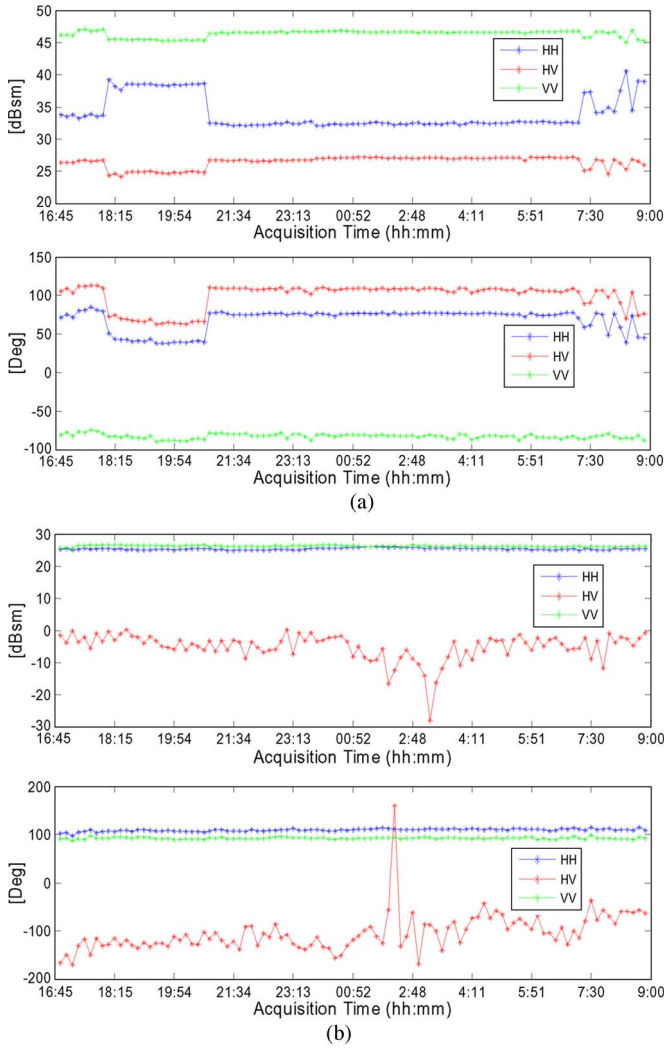

Fig. 4. Time evolution of the amplitude A [dB] and absolute phase φ [deg] (a) concerning the target P_1 and (b) the corner reflector C_1 from 5 P.M. on December 18th, 2006 to 9 A.M. next day. The time sampling step is 10 min.

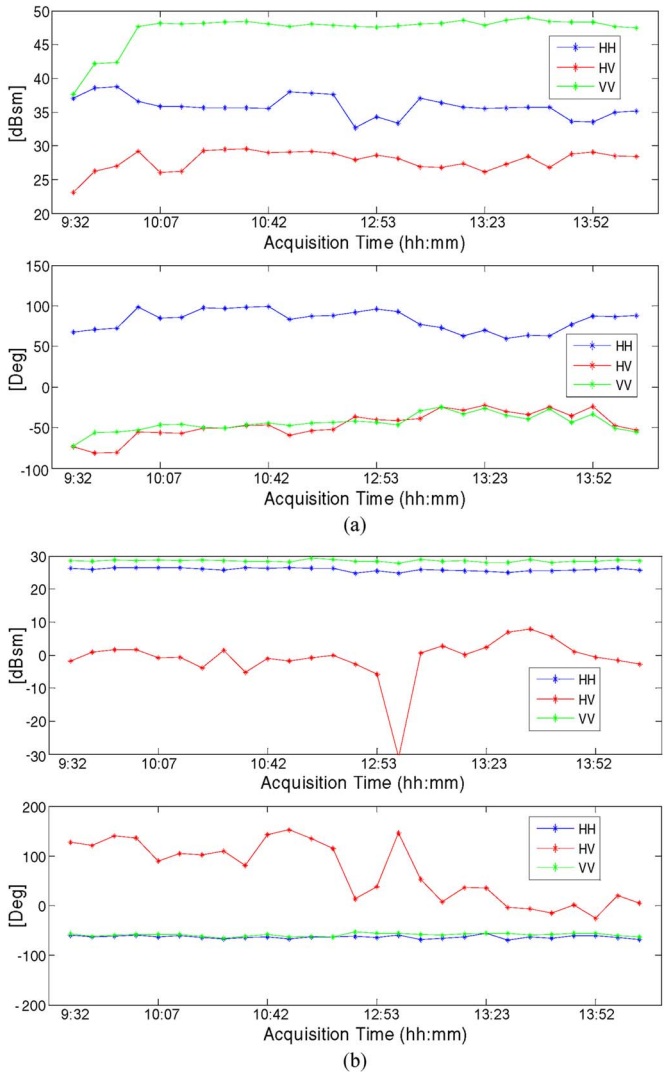

Fig. 5. Time evolution of the amplitude A [dB] and absolute phase φ [deg] (a) concerning the target P_1 and (b) the corner reflector C_1 from 9:30 A.M. to 2:04 P.M. on October 20th, 2006. The time sampling step is 20 min.

environment turns out to depend on the part of the day where data were acquired.

In order to stress this unexpected behavior, the collection of December 18th is first taken into consideration. The scanning process was carried out every 10 min, giving the opportunity to look into the targets temporal evolution in great detail. The plots of Fig. 4(a) describe the polarimetric behavior of a high reflectivity pixel, hereon denoted with P_1, at 400 m from the sensor. After a very stable initial interval (nine acquisitions), a discontinuity leads to a new stable polarimetric behavior that keeps constant for the next 17 acquisitions; finally, a new discontinuity seems to restore the initial backscattering properties. In the last part of the profiles, significant fluctuations are also observable. Any system failure is excluded by the stable answer of the corner reflector C_1 meant for long-term phase calibration, which was mounted on a concrete pillar at about 650 m from the sensor [Fig. 4(b)]. The slightly difference between C_1 co-polar channels is due to the polarimetric signature of the pillar that sums up to C_1. When a diurnal collection is analyzed, P_1 fluctuations generally increase [Fig. 5(a)] whereas C_1 keeps stable [Fig. 5(b)]. The absolute phase difference of the co-polar channels in the two days is due to the different location of the corner reflector employed for the polarimetric calibration of each set of daily acquisitions [8], [9].

It is worth reminding that the discontinuities observed can be tagged neither as residual atmospheric artifacts nor as coregistration uncertainties. The high spatial correlation length characterizing these error sources should make close pixels present similar trends, but careful analyses revealed it is not the case. This can be observed in Fig. 6(a) and (b), which show the evolution of two pixels P_2 and P_3 belonging to two different buildings located at about 30 m from P_1. A final remark is in order: working out a relation between polarization temporal changes and backscattering mechanism modifications is not straightforward. The nocturnal evolution of the normalized-to-span Pauli's components of P_1 [Fig. 7(a)] and P_3 [Fig. 7(b)] shows that the stability of one polarimetric channel is not sufficient to state that the scattering mechanism within the observed pixel maintains constant in time.

In all these evidences, discontinuous polarimetric temporal profiles are not due to processing-chain overall errors but must

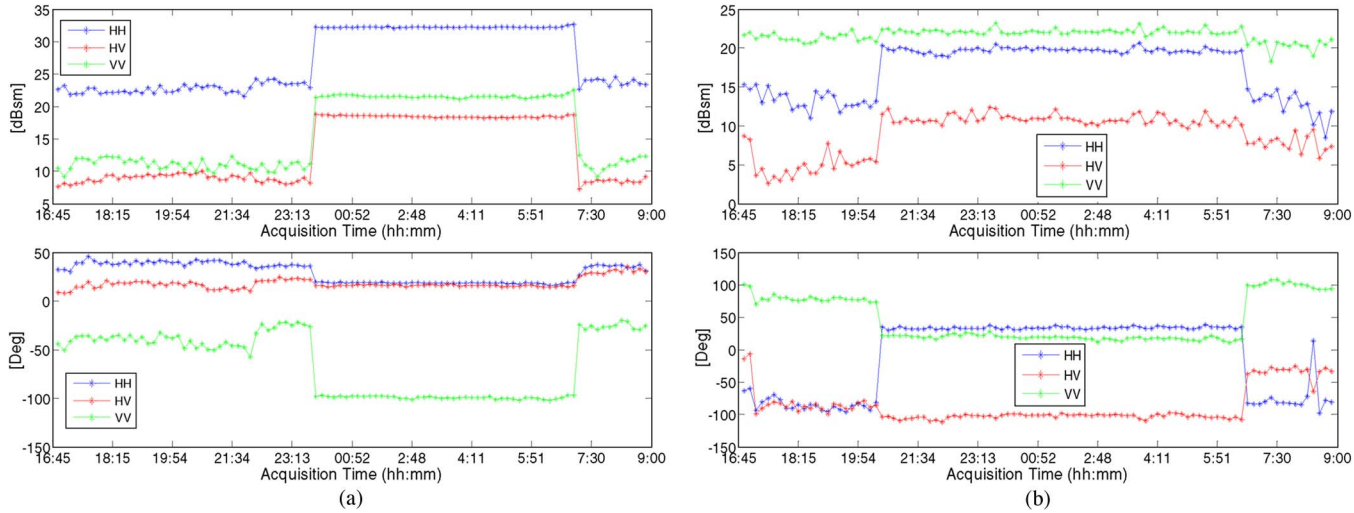

Fig. 6. Time evolution of the amplitude A [dB] and absolute phase φ [deg] concerning two targets (a) P_2 and (b) P_3 located at less than 30 m from P_1 in Fig. 4 during the monitoring activity carried out on December 18th, 2006.

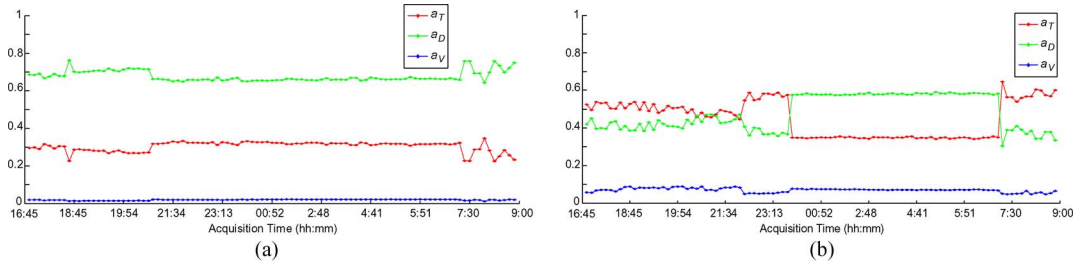

Fig. 7. Time evolution of normalized-to-span Pauli's components concerning the targets (a) P_1 in Fig. 5 and (b) P_3 in Fig. 6 during the monitoring activity carried out on December 18th, 2006.

be explained at the scene level. For this purpose, alternative approaches based on coherent and incoherent analyses of gbSAR daily collections have been considered.

IV. Classical Permanent Scatterers Approach

In Section III, the stability of urban target backscattering at X-band in time was shown to depend on the polarization chosen. For this reason, the first step of the study dealt with the analysis of the temporal evolution of each polarization channel separately. To do this, it was mandatory to employ a procedure that agreed with the main properties of gbSAR acquisition geometry. An assessed method for the detection of stable pixels within urban scenarios in long-term collections of single-polarization satellite data is permanent scatterers (PSs) [14]. This technique is based on the estimation of the dispersion index D_A defined as

$$D_A = \frac{\sigma_A}{m_A} \tag{4}$$

being m_A and σ_A the mean value and the standard deviation of the amplitude samples of the pixel along the image set, respectively. Precise statistical hypotheses allow one to relate D_A to phase dispersion. Essentially, the resolution cell is modeled as a Swerling target of type 1 [1]. When a point target is illuminated at different times (and even from a wide set of incidence angles), the amplitude of the signal backscattered from a PS and affected by additive noise is Rice distributed [15]. For high signal-to-noise ratio (SNR), namely higher than 15 dB, the Rice distribution approaches a Gaussian, and the pixel phase stability σ_φ is related to amplitude dispersion as follows:

$$D_A \simeq \frac{\sigma_n}{A_0} \simeq \sigma_\phi \tag{5}$$

where σ_n^2 is the variance of the circular Gaussian additive complex noise of the signal, and A_0 is the PS complex reflectivity. The larger the number of images, the more reliable the statistical analysis, being the desirable minimum number of scenes around 30. According to simulations described in [14], (5) is valid for D_A lower than 0.25, and it implies a maximum σ_φ of about 14°. Although time scales longer than one day are generally considered, this parameter might be useful for the detection of reliable pixels also in gbSAR acquisitions. Note that the different observation geometry of terrestrial and satellite platforms, which are compared in Fig. 8, does not represent an issue as the statistical hypotheses are exactly the same.

Concerning the area of the Station district in Sallent, a minimum SNR of 25 dB is achieved for pixels belonging to man-made targets. Then, a theoretical D_A in the order of 0.05 is expected. If atmospheric residual errors which may also affect σ_φ are taken into account, the absolute phase dispersion may be rewritten as

$$\sigma_\phi = \sqrt{\sigma_n^2 + \sigma_{atm}^2(r)} \tag{6}$$

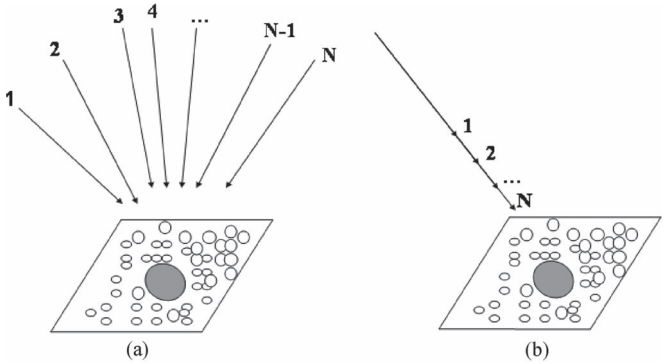

Fig. 8. Multitemporal SAR observations of a PS using (a) satellite and (b) terrestrial platforms. For the sake of clarity, the illuminated target has been modeled as a Swerling target of type 1. Yet, the emphasis is given to variable versus constant observation geometry entailed by the two platforms more than to the hypotheses concerning the statistical distribution of scatterers inside the resolution cell.

TABLE III
CO-POLAR ESTIMATE OF D_A AND σ_φ [RAD] CONCERNING THE TARGET C_1 IN THE CASE OF DIURNAL AND NOCTURNAL MONITORING ACTIVITY

	D_A^{hh} / D_A^{vv}	σ_φ^{hh} / σ_φ^{vv}
Day	0.056 / 0.038	0.055 / 0.054
Night	0.031 / 0.024	0.046 / 0.031

TABLE IV
POLARIMETRIC ESTIMATE OF D_A AND σ_φ [RAD] IN THE CASE OF NOCTURNAL MONITORING ACTIVITY CONCERNING THE TARGETS P_1, P_2, AND P_3. RED NUMBERS INDICATE THE ANOMALOUS CASES

	D_A^{hh} / D_A^{hv} / D_A^{vv}	σ_φ^{hh} / σ_φ^{hv} / σ_φ^{vv}
P_1	0.35 / 0.09 / 0.05	0.25 / 0.28 / 0.05
P_2	0.18 / 0.25 / 0.28	0.06 / 0.23 / 1.30
P_3	0.52 / 0.53 / 0.65	0.17 / 0.09 / 0.56

where the subscript atm denotes the artifacts residual errors contribution, here modeled as a range-dependent parameter [12]. The farther is the target, the higher is the atmospheric phase uncertainty. The estimations of D_A and σ_ϕ over the co-polar responses of C_1 in the diurnal and nocturnal cases (Table III) show that PSs monitored by gbSAR fulfill (5). It is worth recalling the main assumption of PS is that the time samples employed for estimating D_A belong to the same statistical process, i.e., the backscattering process is *stationary* in time. If now the sudden transitions described in Section I are considered, an explanation in terms of additive noise effects is not possible. The reason is twofold. On the one hand, very low values of SNR should be assumed. On the other hand, the statistical properties of the additive white Gaussian noise [15], [16] make the probability to obtain such regular discontinuities practically null.

The hypothesis put forward here is that these effects are instead caused by nonstationary behaviors of urban targets. If D_A and σ_φ from P_1, P_2 and P_3 are estimated over the whole time-sample set, it can be observed that the two quantities do not satisfy (5) (see values in red in Table IV). The reason is that the term A_0 cannot be assumed constant along the observation period. It follows that using the PS technique for detecting stable targets might lead to select unreliable pixels, as for P_1 in the hv polarization, or to cast out pixels carrying stable phase information, as for P_3 in hh and hv polarizations. In conclusion, the statistical model proposed in [14] cannot be directly employed to deal with the urban pixels nonstationary behaviors shown up by gbSAR data sets. A modified approach tailored to the properties of the terrestrial continuous monitoring must be hence worked out.

V. MODIFIED PSS APPROACH

The response of a time-invariant deterministic target in an atmosphere-compensated collection of gbSAR daily acquisitions is mainly affected by additive noise. Despite urban scatterers are generally included in this category, the Section III showed that sudden changes may affect the polarimetric stability of man-made environments. The backscattering stationarity hypothesis fails when anomalous transitions are observed, so that any statistical analysis based on this assumption turns out to be unsuitable. For this reason, an alternative single-polarization technique is here proposed.

The rationale is to split the sequence of daily samples into non-overlapping subsets where the variations of amplitude and phase quantities keep lower than fixed thresholds, i.e., where the scattering process may be assumed stationary in time. The final result is a set of disjoint subsets ordered by cardinality that describe the different time-stationary behaviors that the target showed during the observation period. The subset with the highest cardinality is assumed to provide the most reliable description of the target. Equation (5) does not hold anymore so that amplitude and absolute phase stability must be studied separately. Being the amplitude more robust to target modifications [14], its information is analyzed first.

Let $a_{k,i}^w$ denote the ith amplitude sample in dB of the k polarization channel of $\widehat{[S']}_i^w$ measured by the gbSAR sensor during the day w. In addition, let Th_A define a generic maximum amplitude discontinuity threshold. The daily information of each pixel of the image may be expressed as

$$A_k^w = \{a_{k,1}^w, \ldots, a_{k,N_w}^w\} = \bigcup_{i=1}^{N_k} A_{k,i}^w \tag{7}$$

where $A_{k,i}^w = \{a_{k,m}^w \in A_k^w / |a_{k,i}^w - a_{k,m}^w| \leq Th_A\}$ and $\bigcup$ denotes the set union operator. Note that the term $A_{k,i}^w$ contains essentially the elements of A_k^w whose absolute distance from the reference sample $a_{k,i}^w$ is lower than Th_A. It follows that the subsets $A_{k,i}^w$ are non-disjoint subsets of A_k^w and some of them might be even equivalent. Denoting with # the cardinality set operation and with $I_{w,1} = \{1, \ldots, N_w\}$ the set containing the indices of day w samples, subset useless repetitions are eliminated by defining the first stationary subset $B_{k,1}^w$ of A_k^w as

$$B_{k,1}^w = A^w_{k,\min\left\{i \in I_{w,1} / \#A_{ki}^w = \max\limits_{j \in I_{w,1}} \#A_{k,j}^w\right\}} \tag{8}$$

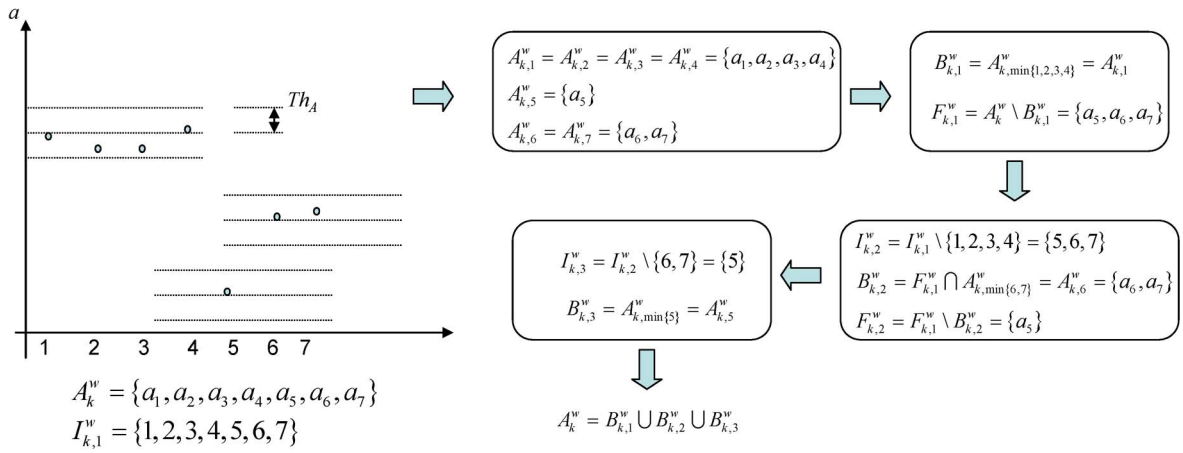

Fig. 9. Sketch of the selection procedure splitting the pixel's collection of gbSAR amplitude samples $A^w_{k,1}$ acquired on day w in the polarization channel k into regular disjoint subsets $B^w_{k,i}$ fulfilling the time-stationary condition derived from the PS formulation.

where "max" operator makes it possible to detect the subset A^w_{ki} with the highest number of elements, while "min" operator is introduced to solve possible equal-cardinality cases. Denoting with "\" the set difference operator, the complementary set of $B^w_{k,1}$ in A^w_k is given by

$$F^w_{k,1} = A^w_k \setminus B^w_{k,1}. \tag{9}$$

The other disjoint subsets $B^w_{k,m}$ of A^w_k are iteratively provided by

$$\begin{cases} I_{w,m} = I_{w,m-1} \setminus \left\{ j \in I_{w,m-1} / a^w_{k,j} \in B^w_{k,m-1} \right\} \\ B^w_{k,m} = F^w_{k,m-1} \cap A^w_{k,p} \\ F^w_{k,m} = F^w_{k,m-1} \setminus B^w_{k,m} \end{cases}$$
$$p = \min \left\{ i \in I_{w,m} / \#\left(A^w_{k,i} \cap F^w_{k,m-1}\right) = \max_{j \in I_{w,m}} \#\left(A^w_{k,j} \cap F^w_{k,m-1}\right) \right\}. \tag{10}$$

The iterative procedure continues until it fulfilled the condition

$$\bigcup_{i=1}^{M_{w,k}} B^w_{k,i} = A^w_k \tag{11}$$

where $M_{w,k}$ is the number of disjoint subsets that reconstruct A^w_k when the disjoint union set operator $\cup$ is applied. Essentially, this formulation joins all the consecutive and non-consecutive samples describing a specific amplitude behavior of a target within the whole observation period. The sub-segment $A^w_{k,1}$ containing the highest number of samples is assumed to represent the pixel more likely behavior. A simple example resuming the basic steps carried out by the iterative selection technique is shown in Fig. 9 for a group of seven acquisitions.

After selecting the k-polarization samples satisfying amplitude stability criterion, the phase information is considered. In order to filter out significant phase discontinuities, a threshold Th_ϕ is defined. The set $\Phi^w_{k,1}$ containing the phase information of the samples defined by $B_{w,1}$ can be expressed as

$$\Phi^w_{k,1} = \bigcup_{n=1}^{\#B_{w,1}} \Phi^w_{k,1,n} \tag{12}$$

where $\Phi^w_{k,1,n} = \{\varphi^w_{k,1,m} \in \Phi^w_{k,1} / |\varphi^w_{k,1,m} - \varphi^w_{k,1,n}| \leq Th_\varphi\}$. The idea described for the amplitude parameter is now applied to the absolute phase, yielding

$$\bigcup_{i=1}^{M_{w,k,1}} C^w_{k,1,i} = \Phi^w_{k,1} \tag{13}$$

where $C^w_{k,1,i}$ define the $M_{w,k,1}$ disjoint subsets that reconstruct $\Phi^w_{k,1}$ ordered by cardinality. Similarly, the phase stability procedure can be applied to the rest of $I_{w,m}$ index subsets. The process finishes when the whole set of phase samples is obtained as union of disjoint subsets. The existence of a subset of amplitude and phase samples with cardinality higher than $N_w/2$ labels the pixel as useful for the subsequent analysis.

In order to interpret the selected subset as representative of a backscattering stationary process, Th_A and Th_ϕ are fixed to

$$\begin{aligned} Th_A &= 2dB \\ Th_\phi &= 10^\circ. \end{aligned} \tag{14}$$

Note that the values chosen for the two thresholds are more constraining than the condition suggested in [14], as $D_A = 0.25$ would mean $Th_A \simeq 8$ dB and $Th_\phi \simeq 14^\circ$ for $SNR_{\min} = 30$ dB. It is worth pointing out that the selection criterion is polarization independent, so that it can be applied to all the elements of $[S]$ separately. The results obtained for P_1 and P_2 are shown for day 7 ($w = 7$) in Fig. 10. Regarding P_1, it is possible to select a useful subset from each polarimetric channel. However, since the profile regularity is polarization dependent, the samples corresponding to each stationary subset might be different. For instance, the whole vv profile gets through the amplitude and phase stability criteria, meaning that the projection of the dominant scattering behavior within the pixel on this polarization is time-stationary ($\#C^7_{vv,1,1} = N_7$). Contrarily, its

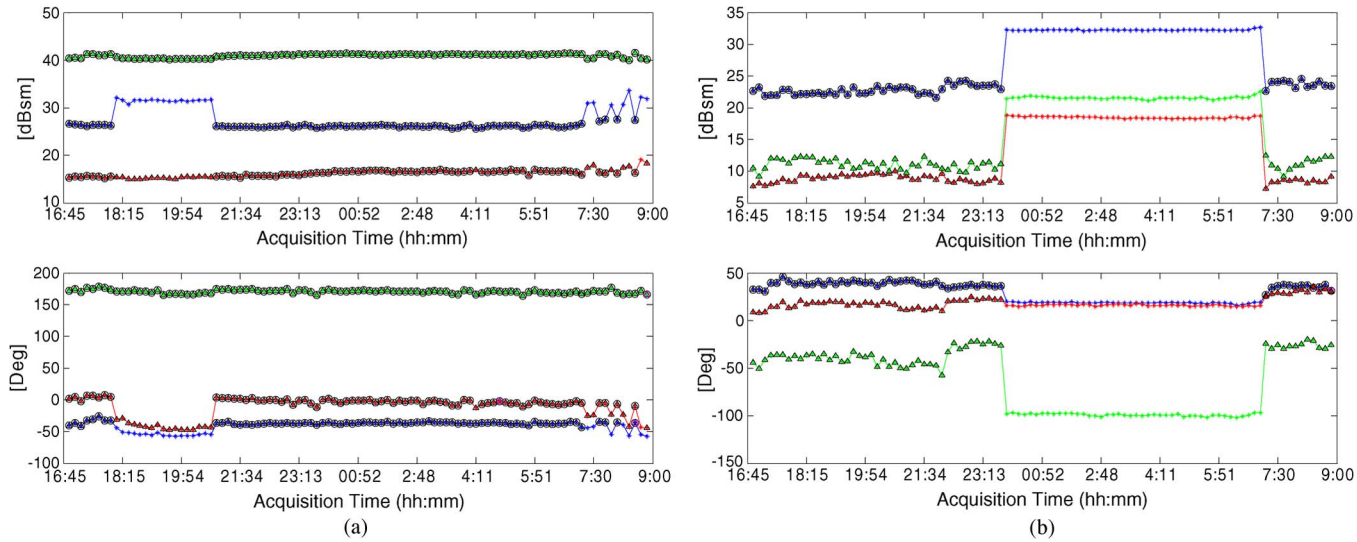

Fig. 10. Time-stationary amplitude $(B^7_{hh,1}, B^7_{hv,1}, B^7_{vv,1})$ and absolute phase $(C^7_{hh,1,1}, C^7_{hv,1,1}, C^7_{vv,1,1})$ subsets selected within the temporal polarimetric profiles of the targets (a) P_1 and (b) P_2. The Δ and O label a sample fulfilling the amplitude and phase stability criteria, respectively. $Th_A = 2$ dB and $Th_A = 10°$ have been used for the selection. Note that for P_2, it results $\#C^7_{hh,1,1} = \#C^7_{hv,1,1} = 0$.

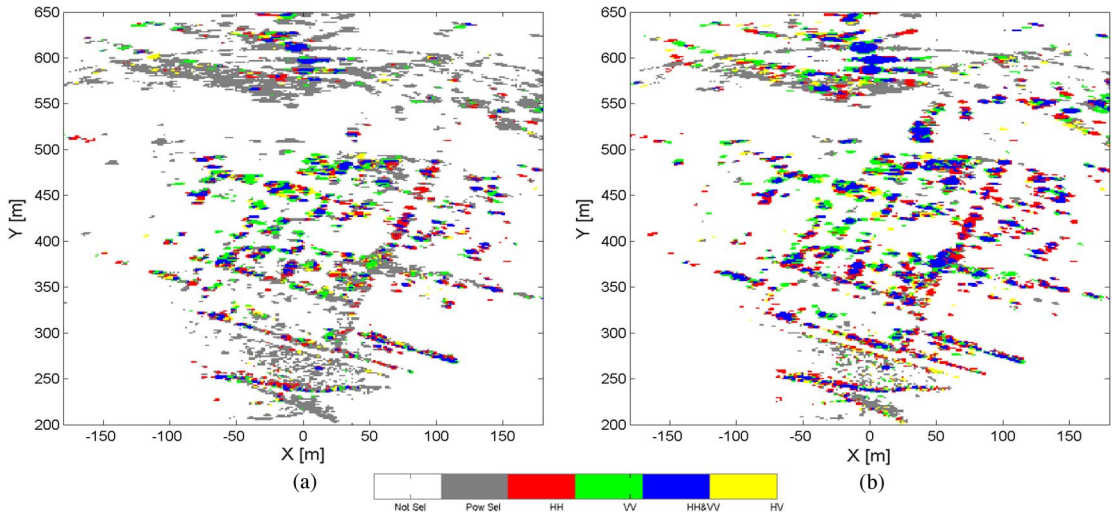

Fig. 11. Polarimetric analysis of pixels fulfilling the condition $\#C^w_{k,1,1} \geq N_w/2$ in the (a) diurnal and (b) nocturnal monitoring activities carried out on 20/10/06 and 18/12/06, respectively. Gray color indicates the pixels fulfilling only the amplitude stability criterion at least in one channel, blue color the pixels fulfilling both amplitude and phase criteria in the two co-polar channels, red, green, and yellow colors denote the pixels getting though the two criteria just in the hh, vv, or hv channel, respectively. The selection thresholds are $Th_A = 2$ dB, $Th_\varphi = 10°$. Minimum amplitude thresholds of 5 dB for hh and vv and -2 dB for hv have been also used to stress the man-made structures.

projection on the other two channels is less stabile, leading to a lower number of useful samples $(\#C^7_{hh,1,1}, \#C^7_{hv,1,1} < N_7)$. Concerning P_2, just the vv channel is labeled as stable. In fact, despite $\#B^7_{hh,1}, \#B^7_{hv,1} > 0$, it results $\#C^7_{hh,1,1}, \#C^7_{hv,1,1} = 0$. As a matter of fact, P_2 hv profile presents an important absolute phase discontinuity that cannot be detected by an amplitude-based criterion.

The study can be now extended to the whole area of interest. The result obtained for the three polarimetric channels within the Station district during diurnal and nocturnal monitoring activities are displayed in Fig. 11(a) and (b), respectively. As already pointed out by Pauli's decomposition (Fig. 3), the backscattered power is mainly distributed along the diagonal of $[S]$. This is mainly due to the building orientation with respect to the synthetic aperture alignment. For this reason, a specific category, the blue one, has been used for describing the pixels meeting the amplitude and phase regularity conditions in both co-polar channels. The red, green, and yellow colors indicate the case the stability conditions are fulfilled just by hh, hv, or vv channel, respectively. Gray points fulfill only the amplitude criterion at least in one channel. Finally, the white background is made up of pixels that do not get through the amplitude test in any polarimetric channel or that show a too low amplitude mean value. As the hv generally shows a very low backscattering power level, the minimum power requirement was fixed 7 dB below the co-polar threshold.

A quantitative description of the same result is given in Table V. For each co-polar channel, the number of pixels selected by amplitude criterion (black) and of pixels that also got through the phase condition (blue) is reported. The use of union

TABLE V
PIXEL SELECTION: DIURNAL VERSUS NOCTURAL MEASUREMENTS. THE AMPLITUDE IS THRESHOLD $Th_A = 2$ dB WHEREAS THE PHASE THRESHOLD IS $Th_\varphi = 10°$

Time/Pol	hh A/φ	hv A/φ	vv A/φ	$hh \cap vv$ A/φ	$hh \cup vv$ A/φ	$hv \backslash hh \cup vv$ A/φ
DAY	6629 3098	3513 1731	7268 3108	3812 1552	10085 4654	1404 535
NIGHT	7206 6023	4610 3543	6478 5322	3838 3126	9946 8219	1722 1342

and intersection set operations demonstrates that combining hh and vv channels makes the number of stable points increase about 50% with respect to the single-polarization selection, meaning that the information each co-polar channel carries is complementary. Concerning the hv polarization, the number of stable pixels is much lower. Yet, this channel might be exploited in order to enhance the quality of the district description by recovering pixels that turn out to be unstable in the co-polar channels. The last conclusion drawn from both qualitative and quantitative analyses is that the urban area behaves differently in nocturnal and diurnal observations. The number of pixels fulfilling the amplitude stability condition is approximately the same in both cases. Yet, only 15% is then discarded by phase selection during the night, while the percentage rises to 50% when the diurnal collection is studied. This trend has been confirmed by the rest of day and night collections. In conclusion, it possible to infer that the polarimetric instability shown by urban targets is explainable in terms of dynamic configuration that this type of scenario may assume during a whole day. Since its scattering properties are more mutable during the day than the night, the daily human activity represents the most plausible cause for nonstationary urban backscattering process.

VI. SHORT-TERM TEMPORAL ENTROPY H_T

The daily evolution of urban scatterers studied in Section V made it possible to stress the contrasting night/day backscattering properties of the urban environment of Sallent. Polarization channels turned out to be affected by target changes differently and hence to carry complementary and not redundant information. Yet, to make out if the polarization channel instability induces also a modification of the dominant scattering mechanism within the resolution cell, fully polarimetric information must be studied jointly. A general and assessed descriptor for the degree of backscattering randomness is the polarimetric entropy H [17], defined in the monostatic case as

$$H = \sum_{i=1}^{3} -P(\lambda_i)\log P(\lambda_i) \quad P(\lambda_i) = \frac{\lambda_i}{\sum_{j=1}^{3}\lambda_i} \tag{15}$$

where λ_i are the eigenvalues of the coherency or covariance matrices, usually indicated as [T] and [C], respectively. By construction, H varies from 0 to 1. The lack of temporal sequence of satellite or airborne zero-baseline PolSAR data limited H estimation to the spatial domain under ergodicity and spatial-stationarity hypotheses for the scattering process. A widely shared interpretation relates H to the spatial presence of multiple and orthogonal scattering mechanisms. Very low values denote the presence of a dominant mechanism. As its value increases, it is usually inferred that more mechanisms spatially coexist in the area the average operation is extended to. For all these reasons, the statistical meaning of H makes this descriptor particularly suitable to deal with natural targets. When urban zones are observed, the deterministic nature of this type of environment provides very low values for entropy, or at least this is expected as far as stationarity hypothesis is fulfilled. When low-medium H values are obtained over urban areas, it is generally assumed that the spatial average was likely extended to pixels belonging to different deterministic targets, and that the information mixing made the entropy global value increase.

With respect to space- and airborne PolSAR data, gbSAR acquisition in Sallent provides a new dimension to play with: the time. In other terms, it becomes possible to estimate H in the time domain without degrading the image spatial resolution.

Being N_w the number of scattering matrices describing the behavior of a pixel during the day w and $[\Psi_P]$ Pauli's set of orthogonal 2×2 complex matrices, it is possible to estimate a time coherency matrix $[T_t]$ as

$$\begin{aligned}[T_t]_w &= \sum_{i=1}^{N_w} \vec{k}_P^{w,i} \cdot \left(\vec{k}_P^{w,i}\right)^\dagger \\ &= \sum_{i=1}^{N_w} V\left(\widehat{[S']}_i^w [\Psi_P]\right) \cdot V\left(\widehat{[S']}_i^w [\Psi_P]\right)^\dagger \end{aligned} \tag{16}$$

where V and $\dagger$ stand for the matrix trace and the vector transpose-conjugate operators, respectively. As $[T_t]_w$ is Hermitian semipositive by construction, it can always be decomposed as follows:

$$[T_t]_w = \sum_{i=1}^{3} \lambda_i^t \vec{u_i^t} \vec{u_i^t}^\dagger \tag{17}$$

where λ_i^t and u_i^t are the eigenvalues and unitary eigenvectors of $[T_t]_w$, respectively. Then, the temporal entropy H_T is directly obtained by substituting the terms λ_i^t in (15).

Taking into account the perfect zero-baseline configuration of the gbSAR sensor, possible spatial inhomogeneities are excluded. It follows that under the hypotheses of ergodicity and time-stationarity, the matrix $[T_t]_w$ describing the scattering process from an urban environment is expected to present a rank close to 1, which means a value of H_T close to zero. In case of nonstationary behaviors of the target, the dominant scattering mechanism within the resolution cell varies along the time axis and the rank of $[T_t]_w$ increases. Accordingly, H_T represents a polarimetric descriptor naturally sensitive to nonstationary properties of the backscattering process.

In order to demonstrate this, simulations are first presented. The maximum number of degrees of freedom of [S] associated with a point target in the monostatic case is six, corresponding to the three amplitude and three absolute phase quantities [18]. For the sake of clarity, a simplified case where only a sudden discontinuity affects one phase term was examined. The phase

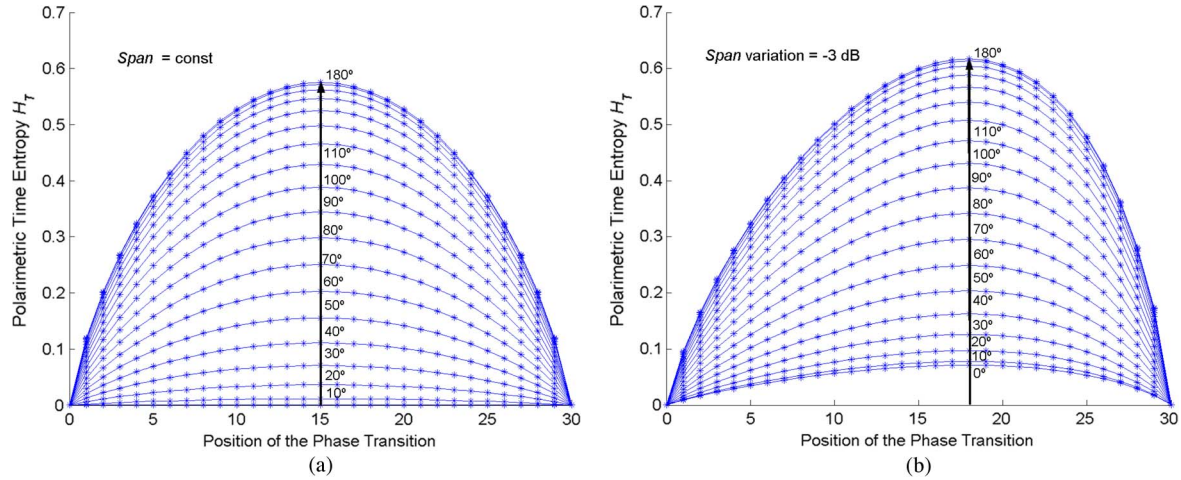

Fig. 12. Study of the variation of the time-entropy H_T induced by a phase jump $\Delta\varphi = 10°$ affecting only one polarization channel (a) and by a combination of amplitude and phase jumps (b) over a set of 30 samples. In the two images, the phase discontinuity goes from 0° to 180° and its position varies from the first to the last samples along the x (*time*) axis. Contrarily, the amplitude discontinuity in (b) is fixed and equal to −3dB.

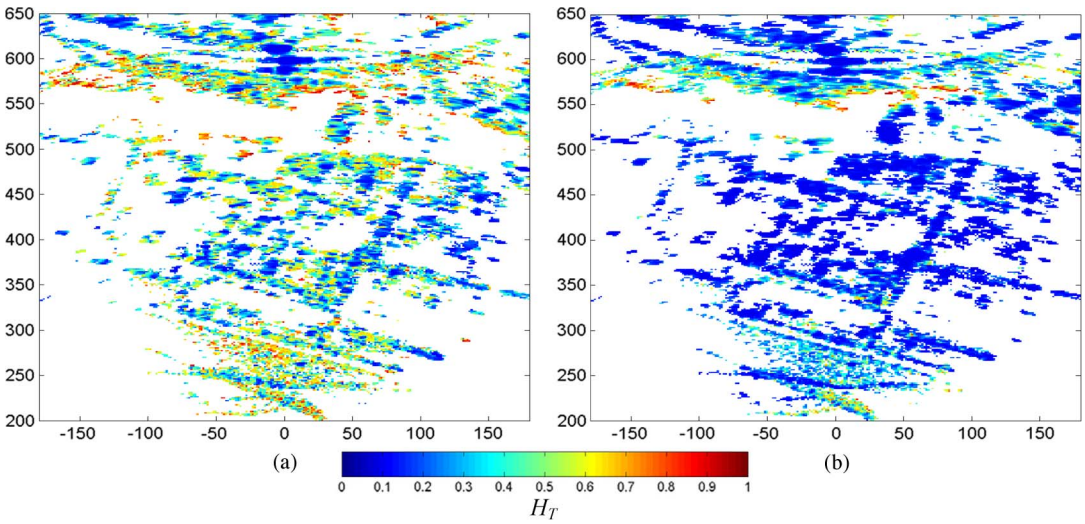

Fig. 13. Distribution of the polarimetric temporal entropy H_T within the Station district of Sallent in (a) the diurnal and (b) nocturnal monitoring activities carried out on 20/10/06 and 18/12/06, respectively. Thirty temporal samples, acquired in about 6 h, have been employed for the estimation of the Coherency matrix $[T_t]$ in both cases.

jump varied in the [0°:180°] range within a set of 30 scattering matrices. The sample where the transition occurs was not fixed in the sequence, but changed gradually from the first to last position. The value of H_T calculated for each discontinuity is shown in Fig. 12(a). The position of the maximum describes the condition of power equality between the two polarimetric behaviors. As the sudden change affects absolute phase terms, the span of [S] keeps constant. The weight of each scattering mechanism in $[T_t]_w$ is then determined by the number of samples before and after the discontinuity. This explains the perfect symmetry of the curves in Fig. 12(a). If the phase discontinuity comes along with an amplitude jump ΔA, the curve becomes asymmetric, and the maximum moves to a new equilibrium position. As example, the H_T behavior in the case a fixed ΔA equal to -3 dB sums to the above-described phase discontinuity is shown in Fig. 12(b). In both images, the worst condition is defined by the 180° phase variation. This is reasonable, since it corresponds to the case the first scattering mechanism turns into a new orthogonal one ($H_T \sim 0.6$).

When two polarizations are affected the same way, the maximum value of H_T decreases. Finally, it becomes negligible when the same discontinuity involves all the polarimetric elements. The reason is that H_T increases only if the transition alters the reciprocal relations among the terms of [S]. If more complex discontinuity configurations are considered, H_T reaches higher values.

Keeping into account the results provided by simulations, it is now possible to interpret correctly the meaning of H_T when it is estimated, pixel by pixel, over real gbSAR zero-baseline time collections. The result obtained with the diurnal and nocturnal measurements analyzed in Section V are shown in Fig. 13(a) and (b), respectively. In order to carry out a meaningful comparison, a set of 30 PolSAR acquisitions selected in a period of about 6 h have been employed. In addition, a common span mask has been applied to focus the attention only on pixels belonging to man-made structures.

In accordance with the results of the coherent analysis of Section V, H_T distribution reveals that a higher number of

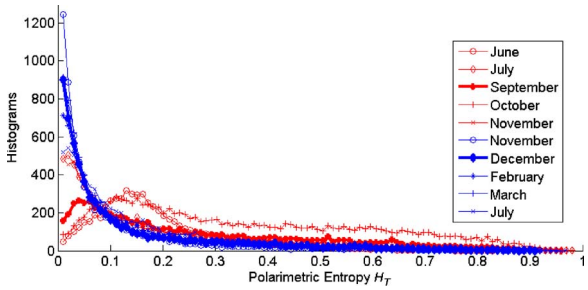

Fig. 14. Histograms of the polarimetric entropy H_T distribution concerning the 10 days of measurements reported in Table II. Red and blue lines denote the diurnal and nocturnal monitoring activities, respectively. The two bulk lines correspond to the two days displayed in Fig. 13(a) (20/10/06) and Fig. 13(b) (18/12/06).

low-entropy pixels are detectable during the night than the day. This conclusion is confirmed by the time-entropy histograms displayed in Fig. 14 corresponding to the days of measurements reported in Table II. For the night case, about 70% of high-reflectivity pixels show H_T values lower than 0.1. During the day, this percentage reduces to 18%. The deterministic nature of scatterers within the district area makes H_T maintain around medium values, although a non-negligible number of pixels (about 20%) show values higher than 0.6.

The results induce again to identify the human activities as the main cause of the urban scatterers' instability. At the same time, the histograms in Fig. 14 confirm the capability of the polarimetric temporal entropy H_T to detect temporal changes in the polarimetric behavior of the deterministic targets.

VII. Urban Environment Long-Term Study

The study carried out in the previous sections dealt with the behavior of high-reflectivity deterministic scatterers at short-term scale. The study of gbSAR daily collections showed that nonstationary backscattering processes may take place within urban environments. Different trends were also found between nocturnal and diurnal collections. Accordingly, the next step of the study is to merge all the samples at disposal and look into a set of long-term measurements.

Nonetheless, some previous comments are in order about polarimetric amplitude and phase. Each set of one-day acquisitions was calibrated as proposed in [8]. Essentially, the technique assumes a diagonal distortion matrix of the sensor and leans on the usage of a calibrator located within the scene. As the corner reflector used for this purpose was positioned within the scenario before starting the acquisition process and removed at the end of the day, specific phase and amplitude offsets must be expected for each daily collection. Amplitude offsets are due to alignment errors. Phase offsets are instead related to the different range position of the calibration and may be defined as

$$\varphi_{0,w} = 2kr_{T,w} \tag{18}$$

where $r_{T,w}$ is the trihedral-to-sensor range distance on day w. The corner reflector C_1 mentioned in Section III, which was meant to provide a long-term stable reference, could not be used to compensate for these differences because of an unexpected long-term instability. The discontinuities shown in Fig. 15

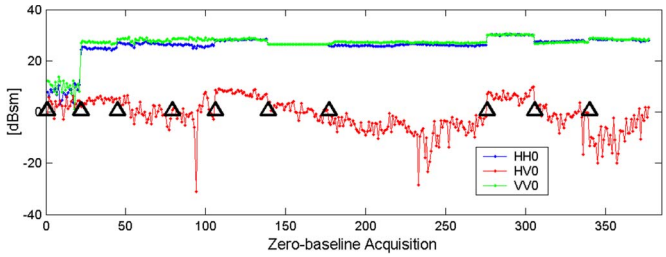

Fig. 15. Polarimetric amplitude profiles of C_1 during the 10 days of measurements reported in Table II. The triangles indicate the first measurement of each day. Note that the reference point is available from day 2 (July 26th 2006).

(a) (b)

Fig. 16. Pictures of the three high reflectivity scatterers selected for the long-time analysis. T_1 (a) is a part of a concrete wall separating the two lanes of the highway close to the urban area. T_2 and T_3 (b) are two close buildings located in the center of the Station district of Sallent.

make the one-day technique of Section V unsuitable to long-term gbSAR data collection. The reason is that they may be misinterpreted as target backscattering changes and, hence, lead to filter out useful time samples. For this reason, a different strategy is pursued.

The problem of amplitude and phase offsets is circumvented by studying the temporal evolution of the normalized-to-span Pauli's components (NPCs) at pixel level. On the one hand, this coherent decomposition is insensitive to absolute phase offsets. On the other hand, the normalization to the span makes it possible to nicely solve any problem related to the amplitude offsets.

Following this idea, the long-term study of the urban environment stability is split into three steps. First, the high complexity of the problem is shown through the analysis of three representative pixels (Section VII-A). Then, the long-term backscattering randomness is characterized by means of H_T (Section VII-B). Finally, a procedure which takes advantage of the coherent and incoherent one-day analysis is put forward to extract stable stationary patterns (Section VII-C).

A. Long-Term Stability

In order to demonstrate the complexity of the analysis to be carried out, three high-reflectivity pixels have been selected. The photographs in Fig. 16(a) and (b) detail the objects the three pixels belong to. The first one is a part of a concrete wall (T_1) separating the two lanes of a highway close to the Station district; the other two targets, T_2 and T_3, are close buildings located in the center of the illuminated area. The temporal evolution of their NCPs is plotted in Fig. 17(a)–(c). The triangles indicate the first sample of each daily collection reported in Table II.

T_1 exhibits a pure single-bounce backscattering behavior that maintained stable during the whole year. Regarding T_2 and

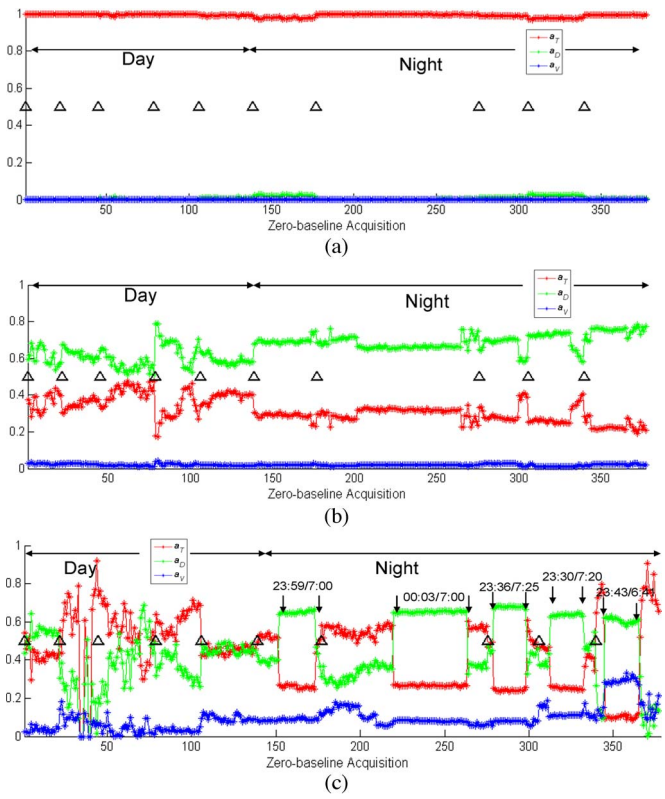

Fig. 17. Long temporal profiles of the normalized-to-span Pauli's components (*NPCs*) concerning the targets (a) T_1, (b) T_2, and (c) T_3 detailed in Fig. 16(a) and (b). The triangles indicate the first sample of the collection gathered during each day of measurements reported in Table II. The black arrows in (c) indicate the time samples delimiting the repeated pattern that T_3 showed during the nocturnal acquisitions.

T_3, a different behavior arises from the diurnal and nocturnal sample sequences. Let T_2 be studied first. During the day, a dominant dihedral-like reflection is observable. Conversely, this behavior may be only partially inferred at some times during the night, where the total power divides up between a_T and a_D with a slow linear variation. The gradualness of the process makes these changes ascribable to atmosphere temperature and humidity daily gradient effects (Appendix A).

Concerning the target T_3, the plots in Fig. 17(c) show a very low diurnal stability: a_T and a_D sometimes invert their role, passing from being dominant to secondary (day 3 and day 4), or become completely chaotic (day 2). During the night, T_3 became very stable, and the presence of a repeated stable pattern is even detectable. The time this change occurred is almost the same every night, as pointed out in Fig. 17(c). This situation may be hardly explained in terms of dielectric constant variations: the transitions are too abrupt and, contrary to what happened for T_2, span value changes in time. These effects are likely to be caused by human habits that periodically modify some property of the target within the resolution cell and consequently its polarimetric scattering response.

B. Long-Term Temporal Entropy H_T Analysis

The estimation of the time-entropy H_T over one-day collections made it possible to stress the higher stability of urban targets during the night than the day. In other words, the likelihood that a dominant scattering from high-reflectivity urban scatterers endures unchanged during a period of at least some hours turned out to be much higher during the night. Thus, low entropy values are expected if H_T is estimated over the union of all the nocturnal measurements, whereas the set of all the diurnal collections are likely to present higher scattering randomness. On the contrary, the results provided by these two studies, which are imaged in Fig. 18(a) and (b), show that long-term diurnal and nocturnal distributions of H_T are very similar. Very few low-entropy pixels located at the same position in both images are detectable. The target T_1, which is marked by a black arrow, is an example. No significant differences are detectable even when H_T estimation is extended to one-year data collection. The histograms plotted in Fig. 19 summarize the long-term backscattering randomness of the urban environment in the three cases.

In order to understand this result, it is worth recalling the physical and mathematical meaning of H_T. In essence, H_T is sensitive to mathematically orthogonal scattering mechanisms contained in $[T]$. Being m and n two PolSAR time samples of a pixel, they contribute to increase the value of H_T if fulfilling the condition

$$\vec{k}_P^{\,n} \cdot \vec{k}_P^{\,m} \ll 1 \tag{19}$$

where $\vec{k}_P$ is Pauli's scattering vector defined in (16). The higher is the number of samples satisfying (19), the higher is the randomness of the scattering process, i.e., H_T. This means that fluctuations as those characterizing the diurnal profiles may have low effects on H_T. Similarly, stable but discontinuous profiles, as the ones observed during the night, may increase the overall value of long-term H_T. The one-day and long-term entropy values of the three targets analyzed in Section VII-A, which are plotted in Fig. 20, come in handy to better understand this issue.

T_1 always shows an almost pure trihedral-like behavior, so that H_T keeps always very low.

T_2 presents fluctuations in time that seem to be independent of time: high values of H_T are obtained for day 3, day 4, day 8, and day 9 are generated by symmetrical profiles of a_T and a_D [Fig. 17(b)]. In the other three days, H_T increases because of the sudden discontinuities between consecutive time-stable scattering behaviors. Finally, the one-year PolSAR information made H_T increase even more, but its value never exceeds 0.2.

Concerning T_3, day 2 and day 9 collections provide the highest level of backscattering randomness. In both cases, this is not caused by response fluctuations but by the difference of NPC profiles with respect to an initial trend. When PolSAR information is merged in two six-month sets, the night time samples provide higher entropy than the diurnal ones, even if the conclusions drawn from the one-day analysis were opposite. The reason is that although the changes make diurnal profiles seem very unstable, a single scattering behavior affected by even noteworthy fluctuations turns out to be less entropic than two different but very stable mechanisms which alternate in time. Yet, even though H_T suggests that the polarimetric information of T_3 is more reliable during the first six months, the extraction of nocturnal time-sample subsets with close polarimetric properties is intuitively more correct.

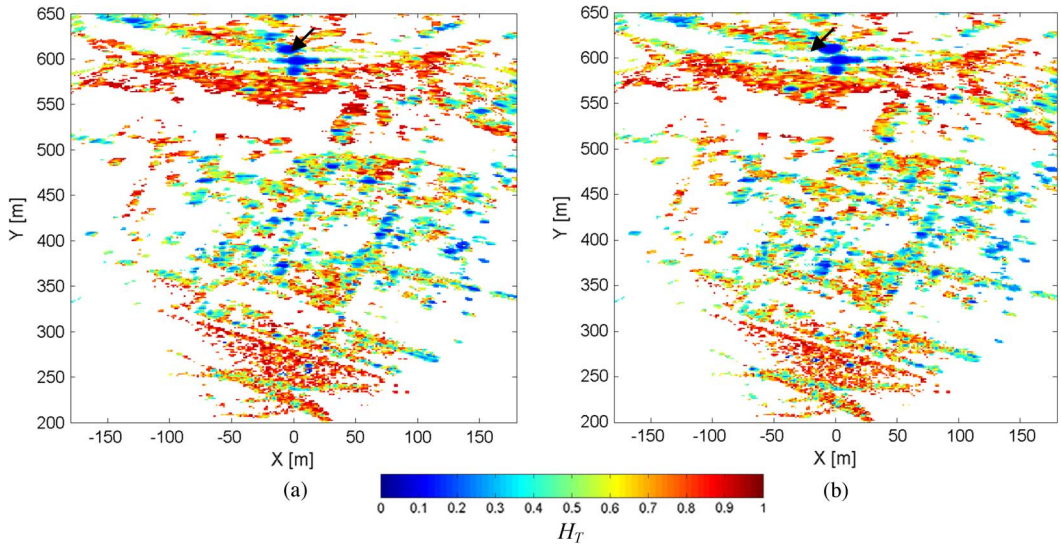

Fig. 18. Time-entropy H_T estimated over six-month (a) diurnal and (b) nocturnal gbSAR acquisitions in Sallent.

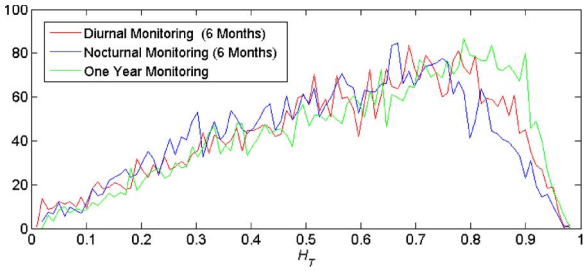

Fig. 19. Histograms of long-time H_T distributions in Sallent.

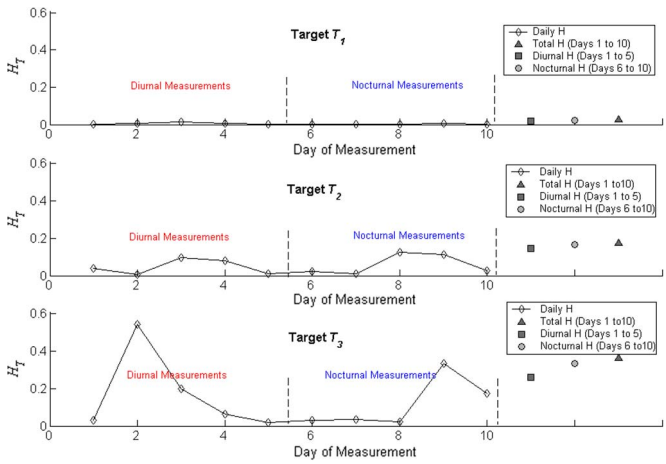

Fig. 20. Time-entropy H_T concerning the targets T_1, T_2, and T_3 calculated using each daily collection of gbSAR acquisitions in Sallent separately, the whole sets of diurnal and nocturnal acquisitions, and all the measurements.

In conclusion, H_T represents a useful descriptor of the degree of backscattering time-stationarity. Nonetheless, a specific filtering procedure able to split long-term PolSAR collections into time-stationary sample subsets minimizing H_T became mandatory.

C. Long-Term Regular Pattern Extraction

In order to cope with the separation of independent time-stationary backscattering processes that alternate in time within the same resolution cell, a three-step methodology is put forward.

The first step is based on the study of the time evolution of NPCs at pixel level. It is worth recalling that NPCs are insensitive to the amplitude and phase offsets. In order to avoid gaps along the pixel temporal description, this procedure must guarantee a minimum number of acquisitions for each day of measurements.

Following the idea described in Section V, the sets of long-term NPCs concerning an illuminated target may be expressed as

$$\begin{aligned} A_T &= \bigcup_{w=1}^{N} A_T^w = \bigcup_{w=1}^{N} \left\{a_{T,1}^w, \ldots, a_{T,N_w}^w\right\} \\ A_D &= \bigcup_{w=1}^{N} A_D^w = \bigcup_{w=1}^{N} \left\{a_{D,1}^w, \ldots, a_{D,N_w}^w\right\} \\ A_V &= \bigcup_{w=1}^{N} A_V^w = \bigcup_{w=1}^{N} \left\{a_{V,1}^w, \ldots, a_{V,N_w}^w\right\} \end{aligned} \tag{20}$$

where A_T, A_D, and A_V denote the trihedral-like, dihedral-like, and volumetric components, respectively; N defines the number of days at disposal; N_w indicates the corresponding number of data sets acquired on day w; $\cup$ stands for the disjoint union set operation. Note that the subsets A_T^w, A_D^w, and A_V^w contain Pauli's components of all the samples acquired during the day w. Let $I = \{1, \ldots, N\}$ be the set of the indices defining the measurement days reported in Table II. Denoting with Th_P the maximum discontinuity threshold along the NPC profiles, A_T may be expressed as

$$A_T = \bigcup_{w=1}^{N} \bigcup_{i=1}^{N_w} A_{T,i}^w \tag{21}$$

where $\bigcup$ indicates the set union operator, and each subset $A_{T,i}^w$ is given by

$$A_{T,i}^w = \left\{a_{T,m}^k \in \underline{A}_T / \left|a_{T,i}^w - a_{T,m}^k\right| < Th_P\right\} \quad \forall k, w \in I. \tag{22}$$

Essentially, each subset $A^w_{T,i}$ contains all the elements $a^k_{T,m}$ of the trihedral-like one-year profile whose absolute distance from the reference sample $a^w_{T,i}$ is lower than Th_P. Note also that $A^w_{T,i}$ are non-disjoint subsets of A_T and some of them may be equivalent. Let $B_{T,1}$ define the most likely fraction of pixel span characterized by an odd-bounce backscattering behavior. According to (21) and (22), $B_{T,1}$ corresponds to the subset $A^w_{T,i}$ that shows the maximum cardinality and, at the same time, guarantees a minimum of $n_{\min}$ samples for each day of measurements. These two conditions may be mathematically described as follows:

$$B_{T,1} = A^w_{T,j} / \left[\#A^w_{T,j} = \max \#A^k_{T,i} \wedge \#\left(A^w_{T,j} \cap A^k_T\right) \geq n_{\min} \right] \quad (23)$$

where $\wedge$ indicates the AND logical operator. The complementary set of $B_{T,1}$ in A_T is given by

$$F_{T,1} = A_T \setminus B_{T,1}. \quad (24)$$

In order to check the existence of other useful subsets fulfilling the requirement stated by $n_{\min}$, the selection process may be iteratively applied to the remaining elements of the trihedral-like temporal profile as follows:

$$\begin{cases} F_{T,n} = F_{T,n-1} \setminus B_{T,n} \\ A^w_{T,i} = \left\{ a^k_{T,i} \in F_{T,n} / \left| a^w_{T,i} - a^k_{T,m} \right| < Th_P \right\} \\ B_{T,n+1} = A^w_{T,j} / \\ \left[\#A^w_{T,j} \max \#A^w_{T,i} \wedge \#\left(A^w_{T,j} \cap A^k_T\right) \geq n_{\min} \right]. \end{cases} \quad (25)$$

The iterative process stops when $B_{T,n+1} = \{0\}$. If the study is now applied to A_D and A_V, the three Pauli's profiles in (20) may be expressed as

$$\begin{aligned} A_T &= \left(\bigcup_{k=1}^{N_T} B_{T,k} \right) \cup F_{T,N_T} \\ A_D &= \left(\bigcup_{k=1}^{N_D} B_{D,k} \right) \cup F_{D,N_D} \\ A_V &= \left(\bigcup_{k=1}^{N_V} B_{V,k} \right) \cup F_{D,N_V} \end{aligned} \quad (26)$$

where N_T, N_D, and N_V denote the number of disjoint subsets each Pauli's component has been split into by the iterative algorithm. Note that these numbers might be different. For instance, the stability of the dihedral-like component may not assure that no power is being exchanged among the other two mechanisms. This means that the stability of all the three components needs to be verified at once. The indices of the elements acquired on day w and contained in the subsets $B_{T,n}$, $B_{D,n}$, and $B_{V,n}$ are given by the following expressions:

$$\begin{aligned} I^w_{B_{T,k}} &= \left\{ i / a^w_{T,i} \in B_{T,k} \right\} \\ I^w_{B_{D,k}} &= \left\{ i / a^w_{D,i} \in B_{D,k} \right\} \\ I^w_{B_{V,k}} &= \left\{ i / a^w_{V,i} \in B_{V,k} \right\}. \end{aligned} \quad (27)$$

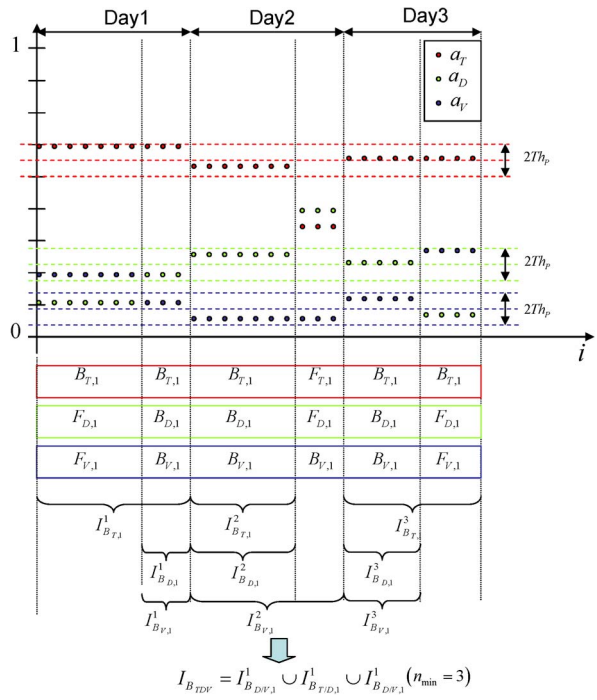

Fig. 21. Sketch of the long-time polarimetric selection based on the simultaneous stability of the three Pauli's normalized components. For the sake of simplicity, just three daily collections and $n_{\min} = 3$ have been considered.

Then, the collection of samples describing the most frequent backscattering process characterizing the pixel under study is given by the set of indices $I_{B_{TDV}}$ defined as

$$\begin{aligned} I_{B_{TDV}} &= \bigcup_{w=1}^{N} \left(I^w_{B_{T,m_1}} \cap I^w_{B_{D,m_2}} \cap I^w_{B_{V,m_3}} \right) \Big/ \\ &\quad \# \bigcup_{w=1}^{N} \left(I^w_{B_{T,m_1}} \cap I^w_{B_{D,m_2}} \cap I^w_{B_{V,m_3}} \right) \\ &= \left[\max_{\substack{k_1 \in \{1,..,N_T\} \\ k_2 \in \{1,..,N_D\} \\ k_3 \in \{1,..,N_V\}}} \# \bigcup_{w=1}^{N} I^w_{B_{T,k_1}} \cap I^w_{B_{D,k_2}} \cap I^w_{B_{V,k_3}} \right. \\ &\quad \left. \wedge \# \left(I^w_{B_{T,m_1}} \cap I^w_{B_{D,m_2}} \cap I^w_{B_{V,m_3}} \right) \geq n_{\min} \right] \end{aligned} \quad (28)$$

where m_1, m_2, and m_3 define the subset of each NCP component which provides the maximum cardinality intersection; the condition "$\wedge$" guarantees that at least $n_{\min}$ samples are selected for each day of measurements. In essence, (28) looks for the three subsets of NPCs which maximize the cardinality of their intersection and, at the same time, guarantee a number of daily common samples higher than $n_{\min}$. The sketch of Fig. 21 shows the subsets $B_{T,1}$, $B_{D,1}$, and $B_{V,1}$ selected by the proposed approach in a simple case of three days of measurements.

At this point, it is worth pointing out that the samples of the three subsets selected by (28) are characterized by very similar polarimetric properties. Yet, the normalized Pauli's components are not sensitive to possible common discontinuities or fluctuations along the amplitude/phase daily profiles, which anyway accounts for a change in the pixel's backscattering process.

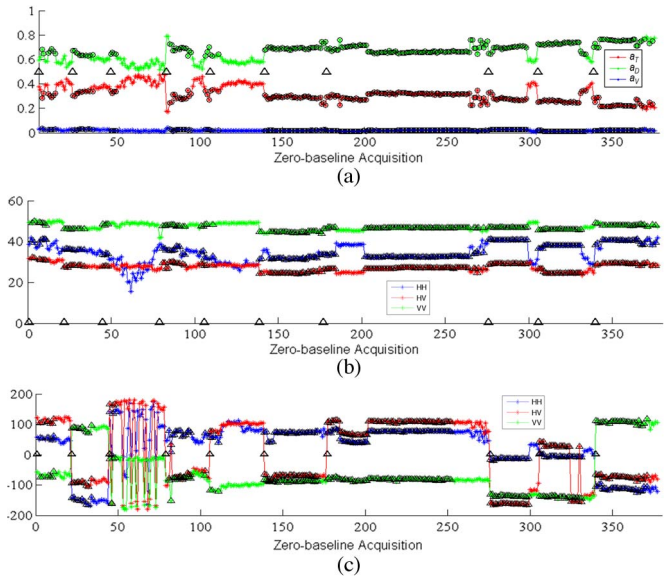

Fig. 22. Long-time polarimetric selection concerning the target T_2. First, the samples belonging to the same stationary process are grouped in $I_{B_{TDV}}$ by studying the stability of the normalized-to-span Pauli's (NPCs) components (a). Then, $I_{B_{TDV}}$ is split into subsets $I^w_{B_{TDV}}$ containing samples belonging to the same day of measurements and the stability of amplitude and absolute phase one-day profiles is checked in the different polarimetric channels separately [small triangles in (b)]. The final set of selected samples $I^{Tot}_{B_{TDV}}$ is provided by the intersection among the day-by-day selection in the three polarimetric channels [dark circles in (c)]. The values of the thresholds used for the filtering procedure are: $Th_P = 0.08, Th_A = 2$ dB, $Th_\varphi = 10°$, $n_{\min} = 4$.

If these discontinuities might be neglected for a polarimetric study, they turn out to be critical for any SAR technique based on the reliability of absolute phase information, as differential SAR interferometry [19].

After performing the polarimetric analysis, it is necessary to prove the stability of amplitude and phase information. To do this, the algorithm described in Section V may be applied to the samples identified by the subsets $I^w_{B_{TDV}}$. The study provides three subsets from each $I^w_{B_{TDV}}$, denoted with I^w_{hh}, I^w_{vh}, and I^w_{vv}, whose intersection provides the indices of the polarimetric-, amplitude- and phase-trustworthy samples acquired on day w. Applying the selection to all the day and afterward the union operator, the one-year span is covered as follows:

$$I^{Tot}_{B_{TDV}} = \bigcup_{w=1}^{N} (I^w_{hh} \cap I^w_{hv} \cap I^w_{vv}) = \bigcup_{w=1}^{N} I^w_{[S]}. \qquad (29)$$

Resuming, the filtering procedure performs a multi-scale analysis. The long-term scale analysis backs up on NPCs to guarantee the stability of the scattering mechanism during the whole observation period. The short-term scale analysis filters out the unreliable samples within each daily collection to preserve the absolute phase information in the three polarimetric channels.

An example of the selection carried out by the three-step procedure when it is applied to the one-year collection of T_2 is shown in Fig. 22. The values of the thresholds used for the selection are: $Th_P = 0.08$, $Th_A = 2$ dB, $Th_\varphi = 10°$, $n_{\min} = 4$. The dark circles in Fig. 22(a) mark the samples given by $I_{B_{TDV}}$ in (28). The small triangles in Fig. 22(b) show the subsets of $I_{B_{TDV}}$ obtained by studying the daily stability of the corresponding polarimetric amplitude profiles separately.

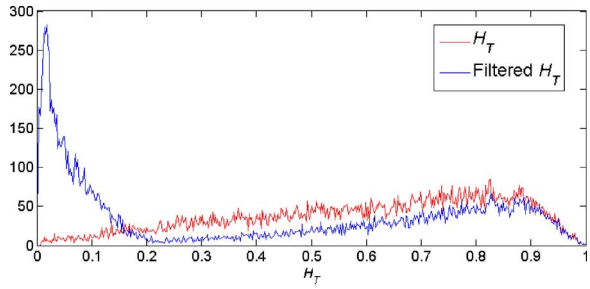

Fig. 23. Histograms of H_T estimated over the (red) non-filtered and (blue) filtered one-year collection of gbSAR data within the Station district of Sallent.

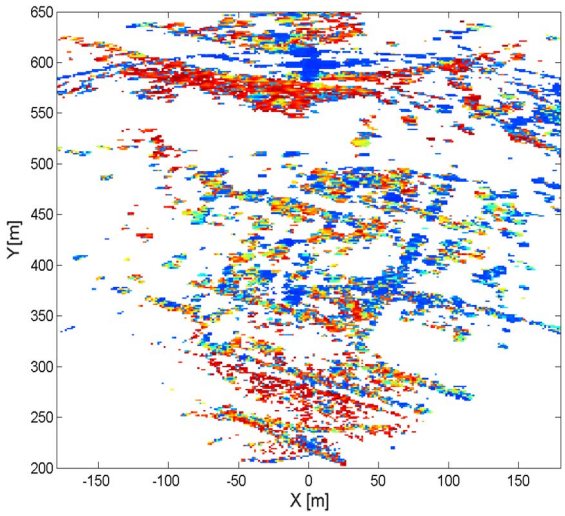

Fig. 24. Time-entropy H_T estimated over the filtered one-year collection of gbSAR data within the Station district of Sallent.

The further application of the phase-stability criterion to each channel of $[S]$ and (29) provide the subset $I^{Tot}_{B_{TDV}}$ whose elements are described by the triangles in Fig. 22(c).

A first demonstration of the effective selection performed by the proposed technique may be achieved using the time-entropy H_T. The two histograms in Fig. 23 show the distribution of H_T within the district area when the estimation is carried out at pixel level over the whole one-year collection (red) and the subset defined by $I^{Tot}_{B_{TDV}}$ (blue). A span minimum threshold equal to 5 dB has been also applied to better describe man-made targets. It can be observed that the selection method here proposed is effective on medium-entropy pixels: they generally pass from an initial value of H_T within the [0.1:0.6] range to a new value lower than 0.1. For instance, the entropy of T_2 in Fig. 22 reduces from 0.18 to 0.012. Concerning the high-entropy pixels, the detection of a subset whose samples fulfill the stability conditions imposed by the selection method is extremely rare. As a matter of fact, the values of histograms for $H_T > 0.85$ are practically identical. This is consistent with the fact the filtering procedure was tailored to the main properties of urban, i.e., deterministic, targets. As it can be observed in Fig. 24, no entropy reduction is obtained over non-deterministic target such as the natural surfaces, for which $I^{Tot}_{B_{TDV}}$ turned out to be empty. In order to avoid any loss of pixels, for these areas, the entropy was estimated over the whole long-term collection of gbSAR acquisitions.

VIII. Conclusion

The one-year measurement campaign driven by the RSLab of UPC in Sallent represents the unique example of long-term monitoring activity carried out using a polarimetric gbSAR sensor in the remote sensing scientific community. The collections of perfect zero-baseline PolSAR data acquired from June 2006 to July 2007 gave for the first time the opportunity to reveal the high complexity of the backscattering process within an urban environment at X-band. The short time-sampling rate of the daily measurements made it possible to stress the polarimetric behavior that man-made structures might present at different time scale. Taking into account the deterministic nature of the observed scene, this was ascribed to nonstationary time behaviors of urban scatterers, which made PS unsuitable for a fruitful analysis. In order to cope with the temporal characterization of the urban test site, an innovative technique able to split nonstationary time-sample sequences into disjoint time-stationary subsets fulfilling PS hypothesis was put forward. A new formulation of the polarimetric entropy in the time domain H_T was also proposed for the detection of scattering process nonstationarities. The main conclusion of the study is that changes in the polarimetric temporal profiles do not always imply a modification of the scattering mechanisms characterizing a pixel. From this point of view, the normalized-to-span components of the Pauli's decomposition (NPCs) represent a useful tool to detect discontinuities in the polarization time evolution.

In order to achieve a reliable characterization of urban pixels within long-term PolSAR data collections, a novel pixel-by-pixel filtering procedure was introduced. Following a multi-scale approach, the regularity of NPCs profiles was used to select samples in each short-term (i.e., daily) collection showing the same long-term polarimetric scattering behavior. This assured that the position of the polarization phase centers within each resolution cell did not change among the different days of measurements, i.e., the polarimetric absolute phase information of each daily subset was preserved at pixel level. The effectiveness of the filtering procedure was finally assessed in terms of reduction of H_T within the district area.

The potential extension of the results presented in this manuscript to spaceborne SAR data needs to be carefully considered. Regarding the acquisition geometry, it has been shown that the gbSAR geometry, characterized by a large incidence angle, makes double bounce be the most important scattering mechanism. In case of space geometry, it may be still expected to be an important scattering mechanism, despite in urban environments, its appearance depends highly on the alignment between the urban structures and the satellite trajectory. As a result, the sensitivity to nonstationary targets in time cannot be excluded in satellite acquisitions. At the same time, satellite data used for amplitude- and coherence-based differential studies are gathered from very close orbits belonging to the same track. This restriction makes the satellite observe an area of interest almost at the same time of the day and with the same incidence angle, allowing one to infer that the probability to experience nonstationary backscattering processes within urban environment becomes low, in particular within nocturnal collections.

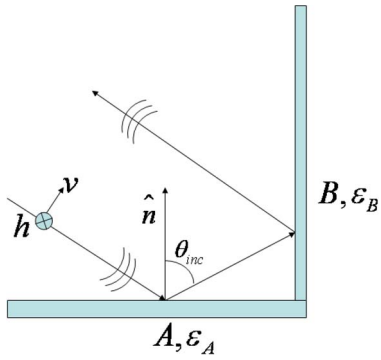

Fig. 25. Sketch of the double-bounce reflection geometry. ε_A and ε_B are the dielectric constant of surfaces A and B, respectively.

Nonetheless, a general conclusion may be drawn from this work. Checking the time-stationarity of the backscattering process within the area to be studied is primary in order to optimize any quantitative information retrieved through long-term SAR data analyses. To this end, polarimetry plays a key role because makes it possible their detection using powerful descriptors as H_T. The filtering procedure here proposed represents a first attempt to cope with the problem of preserving interferometric phase information from nonstationary backscattering. Indeed, this condition turns out to be essential in order to define a new research field where polarimetry and differential interferometry may profitably converge. Future works will be focused on demonstrating the advantages that a fully polarimetric long-term filtering technique provides with respect to single- or dual-polarization measurements for differential interferometric application.

Appendix A

It is notorious that temperature and humidity directly affect the value of target dielectric constant ε [7]. The effect of their changes on the microwave reflection mechanism is almost negligible at medium incidence angles, i.e., for satellite and airborne SAR acquisitions, but it may become significant in gbSAR observation geometries.

Concerning the measurements campaign in Sallent, the observation angle θ ranges from 72° to 82° within the area of interest. Then, it is reasonable to assume that the double-bounce mechanism sketched in Fig. 25 mostly dominates the backscattering from the urban targets. Let ε_A and ε_B be the dielectric constants characterizing the surfaces A and B, respectively. The scattering matrix associated to the reflection process in the BSA convention may be expressed as

$$[S] = \begin{bmatrix} Shh & 0 \\ 0 & Svv \end{bmatrix} = A \begin{bmatrix} R_{hhA} R_{hhB} & 0 \\ 0 & R_{vvA} R_{vvB} \end{bmatrix} \quad \text{(A1)}$$

where the terms

$$R_{hhA} = \frac{\cos\theta_{inc} - \sqrt{\varepsilon_A - \sin^2\theta_{inc}}}{\cos\theta_{inc} + \sqrt{\varepsilon_A - \sin^2\theta_{inc}}}$$
$$R_{hhB} = \frac{\sin\theta_{inc} - \sqrt{\varepsilon_B - \cos^2\theta_{inc}}}{\sin\theta_{inc} + \sqrt{\varepsilon_B - \cos^2\theta_{inc}}} \quad \text{(A2)}$$

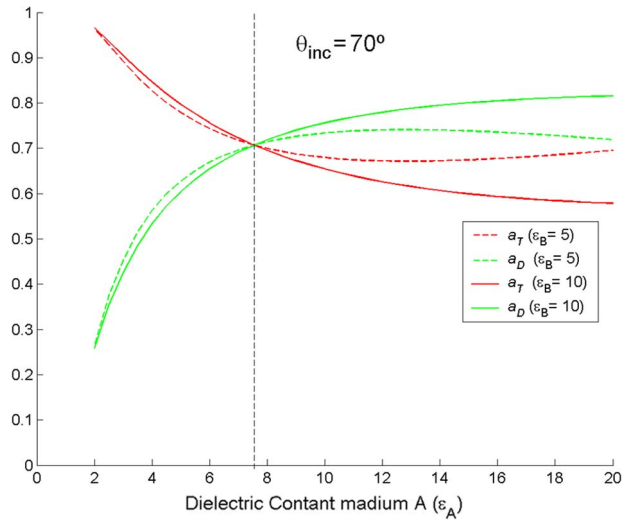

Fig. 26. Behavior of the normalized single-bounce a_T and double-bounce a_D Pauli's components concerning the reflection geometry in Fig. 25 as a function of ε_A and ε_B for $\theta_{inc} = 70°$.

TABLE VI
EXAMPLES OF THE RELATIVE DIELECTRIC CONSTANT ε OF COMMON MATERIALS

	Dielectric Constant ε	
Material	Dry	Wet
Asphalt	[2:4]	[6:12]
Clay	[2:10]	[4:40]
Granite	5	7
Limestone	7	8
Sand	[4:6]	[10:30]
Concrete	[4:10]	[10:20]
Sandy Soil	[4:6]	[15:30]
Clay soil	[4:6]	[10:15]

are the Fresnel coefficients describing the surface scattering process of hh and vv polarized incident waves [7], [15]. Despite the geometry of the problem always generates a double-bounced reflection, it is not sure that the dihedral-like scattering term a_D represents the main component of Pauli.

In fact, the way the total power shares between the trihedral-like and dihedral-like mechanisms at high incidence angle strictly depends on ε_A and ε_B. This can be observed in Fig. 26, where the behavior a_T and a_D is plotted as a function of the two dielectric constants. It can be observed that it is essentially ε_A that modulates the power distribution: the intersection between the two curves, which indicates the changeover point between the two mechanisms, just depends on the incidence angle θ. Denoting its corresponding value ε_A with ε_{ACO}, it can be shown that

$$\tan\theta_{Br} = \sqrt{\varepsilon_{ACO}} \tag{A3}$$

where θ_{Br} is generally referred to as Brewster angle [9]. Examples of the relative dielectric constant values concerning different types of materials in dry and wet conditions are reported in Table VI. In the light of this reasoning, the gradual exchange of energy between the first two Pauli's components of T_2 (Section V) can be explained in terms of modulation of the dielectric constant induced by temperature and humidity gradients. This explanation is confirmed by the fact that in real observation, as well as in simulation, the span quantity is nearly constant. Finally, it is worth pointing out that at high incidence angle, the concept of trihedral-like and dihedral-like mechanisms loses a direct geometrical interpretation. This is the case of T_1, (Section V): its very stable trihedral-like mechanism is likely to be generated by a double-bounce reflection, but, due to the particular observation geometry, it appears as an odd-bounce scattering process.

REFERENCES

[1] M. Skolnik, *Radar Handbook*. New York: McGraw-Hill, 1990.
[2] M. Soumekh, *Synthetic Aperture Radar Signal Processing*. New York: Wiley, 1999.
[3] A. Aguasca, A. Broquetas, J. Mallorqui, and X. Fàbregas, "A solid state L to X-band flexible ground-based SAR system for continuous monitoring applications," in *Proc. IGARSS IEEE Symp.*, Anchorage, AK, Sep. 2004, pp. 757–760.
[4] J. Marturià, O. Mora, D. Xifre, P. Martinez, and A. Roca, "DInSAR techniques versus high topographic leveling surveys: The subsidence phenomena in sallent," in *Proc. ECONGEO*, Barcelona, Spain, Jun. 2006.
[5] P. Blanco-Sanchez, J. J. Mallorquí, S. Duque, and D. Navarrete, "Advances on DInSAR with ERS and ENVISAT data using the coherent pixels technique (CPT)," in *Proc. IEEE Symp. IGARSS*, Denver, CO, Jul. 2006, pp. 1898–1901.
[6] L. Pipia, X. Fabregas, A. Aguasca, C. López-Martínez, S. Duque, J. J. Mallorqui, and J. Marturià, "Polarimetric differential SAR interferometry: First results with ground-based measurements," *IEEE Geosci. Remote Sens. Lett.*, vol. 6, no. 1, pp. 167–171, Jan. 2009.
[7] V. D. Navarro-Sanchez and J. M. Lopez-Sanchez, "Improvement of persistent-scatterer interferometry performance by means of a polarimetric optimization," *IEEE Geosci. Remote Sens. Lett.*, vol. 9, no. 4, pp. 609–613, Jul. 2012.
[8] K. Sarabandi, F. T. Ulaby, and M. A. Tassoudji, "Calibration of polarimetric radar system with good polarization isolation," *IEEE Trans. Geosci. Remote Sens.*, vol. 28, no. 1, pp. 70–75, Jan. 1990.
[9] F. T. Ulaby and C. Elachi, *Radar Polarimetry for Geoscience Applications*. Norwood, MA: Artech House, 1990.
[10] T. Moriyama, S. Uratzuka, T. Umehara, H. Maeno, M. Satake, A. Nadai, and K. Nakamura, "Polarimetric SAR image analysis using model fit for urban structure," *IEICE Trans. Commun.*, vol. E88-B, no. 3, pp. 1234–1242, Mar. 2005.
[11] R. Z. Schneider, K. P. Papathanassiou, I. Hajnsek, and A. Moreira, "Polarimetric and interferometric characterization of coherent scatterers in urban areas," *IEEE Trans. Geosci. Remote Sens.*, vol. 44, no. 4, pp. 971–984, Apr. 2006.
[12] L. Pipia, X. Fabregas, A. Aguasca, and C. López-Martínez, "Atmospheric artifacts compensation in ground-based DInSAR applications," *IEEE Geosci. Remote Sens. Lett.*, vol. 5, no. 1, pp. 88–92, Jan. 2008.
[13] C. Lopez-Martinez, "Multidimensional speckle noise, modelling and filtering related to SAR data," Ph.D. disseration, Univ. Politècnica Catalunya, Barcelona, Spain, Jun. 2, 2003.
[14] A. Ferretti, C. Prati, and F. Rocca, "Permanent scatterers in SAR interferometry," *IEEE Trans. Geosci. Remote Sens.*, vol. 39, no. 1, pp. 8–20, Jan. 2001.
[15] A. Papoulis, *Probability, Random Variables and Stochastic Process*. New York: McGraw-Hill, 1984.
[16] A. B. Carlson, *Communication Systems*, 3rd ed. Singapore: McGraw-Hill, 1986.
[17] S. R. Cloude and E. Pottier, "A review of target decomposition theorems in radar polarimetry," *IEEE Trans. Geosci. Remote Sens.*, vol. 34, no. 2, pp. 498–518, Mar. 1996.
[18] S. R. Cloude, "Group theory and polarisation algebra," *Optik*, vol. 75, no. 1, pp. 26–36, 1986.
[19] R. F. Hanssen, *Radar Interferometry: Data Interpretation and Error Analysis*. Dordrecht, The Netherlands: Kluwer, 2001.

Luca Pipia received the B.S. degree (*cum laude*) in electrical engineering from the Università Degli Studi di Cagliari, Cagliari, Italy, in 2002, and the Ph.D. degree in polarimetric differential SAR interferometry (PolDIInSAR) from the Universitat Politécnica de Catalunya (UPC), Barcelona, Spain, in 2009.

From June 2001 to December 2001, he was with the High-Frequency Institute of the German Aerospace Center (DLR) in Oberpfaffenhofen, Germany, where he worked on land classification using polarimetric SAR (PolSAR) information. From 2003 to 2009, he was with the Remote Sensing Laboratory, Departament de Teoria del Senyal i Comunicacions, UPC, where he was deeply involved in the development and assessment of a novel polarimetric formulation of coherence-based advanced DinSAR techniques using real ground-based PolSAR data. Currently, he is with the Remote Sensing group of the Institut Cartogràfic de Catalunya. His research interests deal with SAR polarimetry, differential SAR interferometry, and more recently, with the retrieval of quantitative information from hyperspectral visible, near- and thermal-infrared airborne data.

Dr. Pipia has served as a reviewer for the IEEE JOURNAL OF SELECTED TOPICS IN APPLIED EARTH OBSERVATIONS AND REMOTE SENSING, the IEEE GEOSCIENCE AND REMOTE SENSING LETTERS, and the IEEE TRANSACTIONS ON GEOSCIENCE AND REMOTE SENSING.

Xavier Fabregas (S'89–M'93) received the B.S. degree in physics from Barcelona University, Barcelona, Spain, and the Ph.D. degree in applied sciences from the Universitat Politecnica de Catalunya (UPC), Barcelona, Spain, in 1995 and 1998, respectively.

In 1990, he joined the Photonic and Electromagnetic Engineering Group, Signal Theory and Communications Department, UPC Barcelona. Since 1996, he has been an Associate Professor with UPC. In 2001, he spent an eight-month sabbatical with the HR Institute of the German Aerospace Agency, Oberpfaffenhofen, Germany. He has published 24 refereed papers in international journals, 75 international conference proceedings, and has received a patent. He is a reviewer in several international journals. His current research interests include radar polarimetry, polarimetric-retrieval algorithms, polarimetric calibration, polarimetric speckle models, ground-based SAR sensors and their applications, and time series for multidimensional SAR data applications for urban and terrain deformation monitoring.

Albert Aguasca was born in Barcelona, Spain, in 1964. He received the B.S. and Ph.D. degrees in telecommunication engineering from the Universitat Politica de Catalunya (UPC), Barcelona, Spain, in 1989 and 1993, respectively.

Since 1995 he has been an Associate Professor at the Telecommunications Engineering School, UPC. His teaching activities involve RF and microwave circuits for communications and radio navigation systems. His main research activities involve the design and development of synthetic aperture radar (SAR) and microwave radiometer systems for UAV platforms. He also collaborates in the design and development of smart antennas and scavenging circuitry. He has published more than 40 papers on microwave SAR and Radiometer systems and microwave circuits.

Carlos López-Martínez (S'97–M'04–SM'11) received the M.Sc. degree in electrical engineering and the Ph.D. degree from the Universitat Politècnica de Catalunya (UPC), Barcelona, Spain, in 1999 and 2003, respectively.

From October 2000 to March 2002, he was with the Frequency and Radar Systems Department, HR, German Aerospace Center, DLR, Oberpfaffenhofen, Germany. From June 2003 to December 2005, he was with the Image and Remote Sensing Group–SAPHIR Team, Institute of Electronics and Telecommunications of Rennes (I.E.T.R.–CNRS UMR 6164), Rennes, France. In January 2006, he joined UPC as a Ramón-y-Cajal Researcher, where he is currently an Associate Professor in the area of remote sensing and microwave technology. His research interests include SAR and multidimensional SAR, radar polarimetry, physical parameter inversion, digital signal processing, estimation theory, and harmonic analysis.

Dr. López-Martinez is an Associate Editor of IEEE JOURNAL OF SELECTED TOPICS IN APPLIED EARTH OBSERVATIONS AND REMOTE SENSING and has served as Guest Editor of the *EURASIP Journal on Advances in Signal Processing*. He has organized different invited sessions in international conferences on radar and SAR polarimetry. He has presented advanced courses and seminars on radar polarimetry to a wide range of organizations and events. He has also received the Student Prize Paper Award at the EUSAR 2002 Conference, Cologne, Germany.